Modeling PPRV pathogenesis in mice to assess the contribution of innate cells and anti-viral T cells

Yashu Sharma[1,5], Roman Sarkar[1,5], Ayush Jain[1], Sudhakar Singh[1], Chander Shekhar[1], ChandraSekar Shanmugam[2], Muthuchelvan Dhanavelu[2], Prabhakar Tembure[3], Rajeev Kaul[4*], Sharvan Sehrawat[1*]

[1]Department of Biological Sciences
Indian Institute of Science Education and Research Mohali
Sector 81, SAS Nagar Knowledge City
PO Manauli Mohali 140306 Punjab India

[2]Division of Virology
Indian Veterinary Research Institute
Mukteshwar UK
[3]Department of Veterinary Microbiology
Nagpur Veterinary College
Nagpur MH 440001

[4]Department of Microbiology
University of Delhi South Campus
Benito Zuarez Road New Delhi 110021

[5]These authors contributed equally to the work. The author order is decided by the seniority of authors.

Running title: Susceptibility and pathogenesis of PPRV in mice.

*Address for correspondence
sharvan@iisermohali.ac.in or rkaul@south.du.ac.in

Conflict of financial interest:

The authors declare no conflict of financial interest.

The study was supported by extramural grant from National Agriculture Science Fund (NASF/ABA-6021/2017-18).

Abstract

We demonstrate a rapid induction of type I IFN response in PPRV stimulated cells and the susceptibility of mice, genetically ablated of interferon response, to PPRV infection. Following PPRV infection, IFNR KO mice gradually reduced their body weights and succumbed to the infection within 10 days. While the infecting inoculum size did not alter the outcome of infection, the nature of the induced disease was qualitatively different. Immunopathological lesions were characterized by the expansion and infiltration of innate immune cells distinctly evident at the lower infecting dose of PPRV infection. The replicating virus particles as well as the viral antigens were abundant in most of the critical organs of PPRV infected IFNR KO mice. Neutrophils and macrophages transported the replicating virus to central nervous system and contributed to pathology while the NK cells and T cells were protective against the virus. Using an array of fluorescently labeled H-2K^{b} tetramers PPRV specific CD8^{+} T cells responses were identified and measured in the infected as well as the peptide immunized mice. Our study therefore established and employed a laboratory animal model for investigating PPRV pathogenesis and the contribution of virus specific CD8^{+} T cells during the virus infection to pave the way for elucidating protective or pathological roles of immune cells during PPRV infection.

Importance

We developed a laboratory animal model for investigating the pathogenesis and immunity induced by PPRV. IFNR KO animals succumbed to the infection irrespective of the dose and the route of infection. Neutrophils and macrophages served as the Trojan horse and helped transport the virus to CNS to cause encephalitis while the NK cells and $CD8^+$ T cells provided the protection against PPRV infection. We additionally identified class I restricted immunogenic epitopes of PPRV in C57BL/6 mice. Our study therefore paves the way for an optimal utilization of this model to unravel PPRV pathogenesis and assessing the host correlates of protection.

Introduction

Peste des petits ruminants virus (PPRV) causes high mortality in herds of small ruminants such as sheep and goats and is responsible for major economic losses to livestock sector in developing countries (1–4). PPRV is a negative sense, single stranded enveloped virus of paramyxoviridae family that also include other members that cause debilitating diseases in animals as well as humans. These include Rinderpest virus (RPV) and Canine distemper virus (CDV) of animals and measles virus (MeV) and mumps virus (MuV) of humans (5, 6). PPRV genomes encode for six structural proteins i.e., nucleocapsid (N), phosphoprotein (P), matrix (M), fusion (F), hemagglutinin (H) and polymerase (L) and two nonstructural proteins, C and V (5). The protective and pathological mechanisms activated by the virus as well as the roles of immune cells in its pathogenesis have not yet been adequately elucidated that is primarily attributed to the unavailability of a laboratory animal model. We therefore investigated PPRV pathogenesis in a more accessible vertebrate laboratory animal model to better understand immunity and immunopathology induced by PPRV.

Currently, a live attenuated prophylactic vaccine against PPRV is used in small ruminants. While the vaccine induces a lasting immunity, a transient immunosuppression is usually evident in vaccinated animals that could enhance their susceptibility to heterologous infections (3, 5). Therefore, it is imperative to study the contribution of cellular and molecular mediators induced by the virus in infected animals to better understand its pathogenesis and help devise improved vaccination strategies should a need arise. This is even more relevant for the contemporary animal health care system as the extensive efforts are made to eradicate PPRV globally. That an intensive vaccination program could help eradicate PPRV is bolstered by the

success achieved in eradicating a related RPV. Therefore, an accessible laboratory animal model for elucidating PPRV pathogenesis is likely to improve our understanding of the induced molecular and cellular mediators. Similarly such a model would shed light on the host correlates of protection.

We demonstrate a rapid induction of type I IFNs (α and β) as well as IFN-γ response in PPRV-stimulated immune cells but the kinetics of response varied depending on the cell types and the dose of the stimulating virus. Mice genetically deficient for IFN response (AG129) succumbed to the infection within ten days irrespective of the dose of inoculum or the route of PPRV infection. The inoculum size altered the pathology qualitatively. A lower infecting dose of the virus induced predominantly an immunopathological response in mice infected with PPRV via intranasal route. The replicating PPRV as well as its antigens were detected in most of the analyzed organs. Innate immune cells such as neutrophils and macrophages likely transported the replicating virus to CNS and elsewhere. A reconstitution of IFNR KO mice with wild type $CD8^+$ T cells conferred a survival advantage during infection, a suggestion for their critical role in the PPRV control. We also identified immunogenic class I ($H\text{-}2K^b$) restricted epitopes of PPRV in mice using epitope prediction tools and demonstrated their immunogenicity *ex vivo* and *in vivo*. Therefore, our study established a laboratory animal model that could be valuable for understanding the immunological and virological parameters of morbilivirus induced diseases.

Materials and Methods

Virus and cells

PPRV vaccine strain Sungri/96 was used for all the *ex vivo* and *in vivo* experiments. The virus was cultured, harvested and titrated using Vero cells and stored at -80˚C till further use as described earlier (4, 7). The infecting dose of the virus was calculated as $TCID_{50}$ values by a previously described method (8). RAW264.7 cells were cultured in complete RPMI medium supplemented with 10% FBS and penicillin-streptomycin in a humidified CO_2 incubator.

Antibodies and other biological reagents

Antibodies used in this study were purchased from BD Biosciences, Tonbo biosciences, BioLegend, and eBiosciences. The antibodies used were against CD4 (clone GK1.5), purified CD16/32 (Clone 2.4G2), CD11b (clone M1/70), Gr1 (clone RB6-8C5), F4/80 (clone T45-2342), CD8 (clone 53-6.7), $H2K^b$ (clone AF6 88.5), mouse IgG, CD45.1 (clone A20), CD45.2 (clone 1O4), CXCR3 (clone 173), CD44 (clone IM7), CD62L (clone MEL 14) and CD45 (Clone 30-F11). All the antibodies were diluted in FACS buffer. Other reagents such as DMEM, RPMI 1640, and penicillin-streptomycin antibiotic were purchased from Lonza. Trypsin, SYBR Green and propidium iodide were obtained from Life Technologies. H&E was from HiPrep, M-CSF was from Peprotech and OCT compound was obtained from Fisher HealthCare. FBS, p-nitrophenol phosphate and Freund's complete and incomplete adjuvant were procured from Sigma-Aldrich.

Generation of bone marrow derived macrophages (BMDMs)

Long bones were collected from sacrificed C57BL/6 mice and sterilized in 70% alcohol. Bone marrows were removed to prepare single cell suspension as described earlier (9). RBCs present in the bone marrow cells were lysed and the bone

marrow cells were cultured in 48 well plates ($1x10^6$ cells/well) in the presence of 10ng/ml M-CSF for 7 days. Media was changed after every two days. The cells were cultured in 10% RPMI (Gibco□BRL, Rockville, MD, USA) supplemented penicillin (100U/mL) and streptomycin (100μg/mL). After 7 days, cells were collected, washed and stained for F4/80 positive and CD11c negative population for phenotypic characterization and for performing further experiments.

Measuring type I and II IFN response in PPRV pulsed macrophage cell line and primary BMDM cells

RAW macrophages and BMDMs were pulsed with PPRV at multiplicity of infection (MOI) of 1 and 10 to measure the kinetics of type I IFNs (α and β) and IFN-γ response by qualitative real time polymerase chain reaction (RT-PCR). Murine macrophages and RAW cells pulsed with replicating PPRV or the inactivated virus and samples were collected at 15 min, 30 min, 1hr and 6hr. The cells were processed for isolating mRNA at different time points. The mRNA was converted into cDNA using a first strand synthesis kit (Verso cDNA synthesis kit, Thermo Fisher Scientific). The expression of hypoxanthine phosphoribosyltransferase 1 (HPRT 1) gene served as an internal control. The relative expression for each gene was calculated by using Δ(ΔCt) method.

Infection of mice with PPRV

All the experiments involving animal experiments were performed strictly in accordance with the protocol approved by the Institutional Animal Ethics Committee, IISER Mohali, constituted under the aegis of committee for the purpose of control and supervision of experiments on animals (CPCSEA). IFNR KO (AG129) and congenic C57BL/6 mice (CD45.1 and CD45.2) were used for *in vivo* experiments. Animals were infected using intraperitoneal (i.p) or intranasal (i.n)

routes with the indicated doses of PPRV. Different physiological parameters such as body weight, body temperature, behavior and the mortality pattern were measured in different groups of animals. For most of the experiments, the animals were sacrificed at the termination of experiments when the body weight for any of the groups dropped by more than 20%. Different lymphoid and non-lymphoid organs were collected to detect the replicating virus, viral antigens, and performing the cellular analysis in lymphoid organs such as spleen, mediastinal LNs as well as non-lymphoid organs such as bronchoalveolar lavage (BAL), lungs and brain tissues. Before collecting organs from different groups of mice, a heart perfusion with 20 ml of PBS was performed to remove any contaminating cells of blood from the collected organs.

Reconstitution of IFNR KO mice with T cells to measure their anti-PPRV functions

In order to measure the protective ability of immune cells, the graded doses of MACS purified $CD4^+$ and $CD8^+$ T cells from C57BL/6 WT mice were adoptively transferred in sex matched IFNR KO animals. The recipient animals were subsequently infected with PPRV. Mice not transferred with any cells served as the control. Recipient animals were observed for their body wight and survival. At the termination of experiments, lymphoid organs of animals were collected for cellular analysis.

Cell purification and adoptive transfer

The different subsets of T cells and innate immune cells such as macrophages, neutrophils, dendritic cells were isolated from C57BL/6 mice either by magnetic cell sorting kits or by FACS sorting. The sorted cells were collected at low temperature in the complete RPMI. The cells were pulsed with PPRV for one hour.

After extensive washings, the cells were counted and the indicated numbers of cells were transferred i.v in IFNR KO mice.

Bioinformatic analysis to predict immunogenic peptides of PPRV

Amino acid sequences of PPRV structural proteins were retrieved from National Centre for Biotechnology Information (NCBI) database in FASTA Formats. The immunogenic peptides for one of the class I MHC molecules of C57BL/6 mice (H-2K^b), were predicted using immune epitope data and analysis resource (IEDB). The software uses artificial network (ANN) and stabilized matrix method (SMM). The percentile rank of <2 and IC_{50} values were selected for the prediction. A low percentile rank and the lower IC_{50} values of <50nM indicated high affinity binders. The peptides with IC_{50} values between 50 and <500nM were considered as intermediate affinity binders while with values >500nM were considered as the low affinity binders (10). Additional parameter for selecting peptides was their immunogenicity scores (11,12). Additionally a percentile rank for the predicted peptides was generated by comparing IC_{50} values of predicted epitopes against a set of random peptides using SWISSPROT database. The selected peptides were commercially synthesized and obtained from GL Biochem. The purity of the synthetic peptides was greater than 90%.

Molecular Docking analysis

For predicting the binding affinities of different peptides for class I MHC molecules (H-2K^b and Caprine Leucocyte antigen, CLA1), molecular docking analyses were performed using HPEPDOCK-web server. Default parameters were used for all the docking experiments as described elsewhere (13). HPEPDOCK server uses a hierarchical algorithm, MODPEP program for a blind protein-peptide docking and generates an ensemble of peptide conformation by considering

flexibility conformation in the respective peptide and the PDB File 1S7Q for the homology modeling with H-2K^b protein. To test the efficiency of docking algorithm, a known immunogenic 9-mer peptide derived from Sendai E virus (SEV) nucleoprotein (FAPGNYPAL) was used for docking with H-2K^b. Since the outcome of docking could be dictated by a potentially problematic algorithm that overemphasize the numbers of interactions rather than the conformation, we referred to the solved crystal structure of a nonameric peptide (SEV-9) with H-2K^b to better predict the results from docking analyses. We then compared the energy parameters of the best-selected structures among different PPRV peptides docked with H-2K^b. To further refine and define the interacting residues both quantitatively and qualitatively, we used molecular modeling program UCSF Chimera for binding analysis (14). As the goal of such experiments was to explore the translational value of such peptides in small ruminants, we superimposed H-2K^b with goat class I MHC (CLA-1) molecule at 1.5A RMSD (root mean square distance) using the tool, Matchmaker, available in the UCSF Chimera. Similarly docking studies were done for CLA-I with different PPRV peptides and the representative docked structures were generated using UCSF Chimera. A comparative analysis between docking scores of H-2K^b and CLA-I for the similar peptides was also performed.

Class I MHC stabilization assays

The stabilization of class I MHC by each peptide was measured using both cellular and acellular assays. TAP deficient murine T cell lymphoma cells (RMA/s cells) were used for determining the peptide induced surface stabilization of class I MHC molecule by flow cytometric analysis as described earlier (15). RMA/s cells were maintained in RPMI (Gibco□BRL, Rockville, MD, USA) supplemented with 10% fetal bovine serum (FBS), penicillin (100U/mL) and streptomycin (100µg/mL).

243 $2x10^5$ cells were serum starved for 3 hrs at 37°C and subsequently pulsed with the
244 respective peptides to induce their surface class I MHC (H-$2K^b$) stabilization. Graded
245 doses of peptides were added in serum free RPMI followed in which cells cells were
246 incubated at 37°C for 7 hrs. The cells were then washed with PBS and stained with
247 anti anti-H-$2K^b$-FITC antibody. Live and dead cells were differentiated using
248 propidium iodide (PI) staining. The cells were analysed by FACS Accuri flow
249 cytometer (BD Biosciences, Breda, The Netherlands). The data is represented as
250 percent positive cells or the mean fluorescence intensities (MFI) for the expression of
251 H-$2K^b$. EC_{50} value for high affinity peptides were then calculated.

252 An acellular assay was also used for determining the class I MHC
253 stabilization as described elsewhere (16). Briefly, ELISA plates were coated with
254 streptavidin overnight at 4˚C. Subsequently, H-$2K^b$ monomers were added to the
255 plates. The monomers were generated by refolding a UV photocleavable ligand,
256 (FAPG(Anp)YPAL), β2 microglobulin and H-$2K^b$ heavy chain followed by their
257 biotinylation as described earlier (15, 17). The unbound H-$2K^b$ monomers were
258 washed and the control and PPRV peptides were added to the identified wells in the
259 plates. The plates were then exposed to UV radiations at 365nM for 30 min to
260 achieve the displacement of UV ligand with respective peptides. The efficiency of
261 exchange was measured by probing the washed plates by adding anti-β2
262 microglobulin antibody. Subsequently, a mouse anti-IgG antibody enzyme conjugate
263 (1:10000) was added after washing the plates. Thereafter, substrate, (p-nitrophenol
264 phosphate (1mg/ml) was added for its conversion into a chromogenic product. The
265 stop solution was used to block the reaction and the plates were measured for
266 absorbance at 405 nm. Positive and negative controls were also included in the study
267 (18).

PPRV infection and peptide immunization of mice for PPRV specific $CD8^+$ T cell analysis

In order to determine the immunogenicity of predicted peptides in vivo, we performed two types of experiments. Throughout the manuscript, plaque forming units (PFU) and focal forming units (FFU) are used interchangeably as clear plaques are not observed when PPRV in grown in Vero cells. In first set of experiments, WT C57BL/6 mice were i.p. infected with a high dose of PPRV ($5x10^6$ PFU). After seven days a second dose of PPRV was given to animals to boost responses. The analysis of the expanded cells was performed three days later by measuring the frequencies PPRV-peptide specific $CD8^+$ T cells by tetramer staining. In second set of experiments, C57BL/6 mice were immunized either with the cocktail of peptide (AILTFLFLL, FMYLFLLGV, FSAGAYPLL and IGLVRDFGL) each with 5µg/mouse in complete Freund's adjuvant subcutaneously. After two weeks, a second injection of the same concentration was administered but emulsified in the incomplete Freund's adjuvant. Three days later the frequencies of peptide specific $CD8^+$ T cells were analyzed by tetramer staining of PBMCs.

Isolation of inflammatory cells from brain tissues and lungs

Inflammatory cells were isolated from the brains and lungs of IFNR KO mice by using protocol as described earlier (19). Briefly, brain tissues were minced into 3-4 mm pieces with a sterile scalpel or scissors under complete aseptic conditions. Washing was done 4-5 times with 10mM PBS. Extra supernatant was removed from tissue pieces container kept on ice. 0.25% trypsin was added to samples followed by their incubation at 4°C for 16 hrs. Then, trypsin was discarded and incubation was done at 37°C for 30 min. Complete RPMI was added to prepare single cell suspension. After washing with PBS, cells were used further for experiments.

Flow cytometry for cellular analysis

Different lymphoid and non-lymphoid organs were collected from infected or immunized mice. The single cell suspensions were prepared from collected organs for cellular analysis. The cells were stained using indicated fluorescent labeled antibodies at cold temperature for 30 minutes. Fc block was done before surface staining. Stained cells were acquired by FACS Accuri or BD FACS Aria fusion. The analysis of the data was performed by Flow Jo software.

Fluorescent microscopy and histological analysis

The organs collected from infected and control animals were stored in OCT compound. Tissue sections of 6□m were cut and dried. The dried sections were first blocked with anti-CD16/CD32 antibodies followed by incubation with anti-PPRV H and N monoclonal antibodies. Anti mouse FITC IgG antibodies were then used as secondary antibodies. The sections were analyzed using a fluorescent microscope and the images were generated by Image J software. Similarly, the tissue section from brain tissues were dried and stained with Hematoxylin and Eosin Y. The sections were analyzed by Leica DMi8 microscope as described earlier (20).

Statistical analysis

Statistics was applied to the data and analysed by using ANOVA, Student t test or the Gehan-Breslow-Wilcoxon test as indicated in the respective figures. Graph Pad Prism v5.03 was used for such analysis. The level of significance was determined as $P < 0.05$ *, $P < 0.01$ **, $P < 0.001$***, $P < 0.0001$****.

Results

PPRV infection induces a rapid interferon response

Interferon response constitutes the first line of an anti-viral defense mechanism. We therefore measured the expression of both type I (α, β) and type II (γ) IFN response in a murine macrophage cell line (RAW macrophages) and the primary BMDMs that were stimulated with a low (1MOI) and high (10MOI) dose of PPRV. A low dose of PPRV as compared to the high dose induced significantly more IFNαin RAW macrophages at 1hr post stimulation (Fig 1A). However, a reverse trend as well as an early induction was observed in BMDMs (Fig 1D). Furthermore, the overall expression levels of IFNα were approximately 100 fold more in the primary BMDMs as compared to those in RAW macrophages (Fig 1A and D). Interestingly, we observed a very rapid induction of IFNα within 15 min of stimulation by primary BMDMs but its expression was evident in RAW macrophages only after 1 hour (Fig 1A and D). Similarly IFNβ expression was only detectable at significant levels in PPRV stimulated RAW macrophages after 1hour (Fig 1B). In stimulated BMDMs, the message of IFNβ was evident albeit at lower levels as compared to that of IFNα (Fig1E). IFNγ was induced at a low infecting dose of PPRV in RAW cells but the primary BMDMs expressed it in significant levels only at the high MOI of PPRV (Fig 1C and F). The heat inactivated PPRV induced the production of both type I and type II IFNs but to a much lesser extent and that too in the early stages of stimulation (Fig S1). These results might suggest that not only the viral genome or its replication intermediates but also some of the PPRV proteins could serve as the PAMPs for inducing IFN responses.

Our results demonstrated that both α and β IFNs were induced in PPRV stimulated cells but the overall expression was dependent on the infecting dose as well as the nature of responding cells. The expression profile of type I interferon (IFNα and IFNβ) also indicated a dichotomy in their function with the IFNα being induced rapidly and in high concentrations but IFNβ was produced later on. Such a response pattern could diversify the IFN response in providing an antiviral state.

Mice genetically depleted of IFNRs are susceptible to PPRV infection

Having demonstrated a rapid induction of IFN response in the PPRV pulsed macrophages; we tested whether or not the mice, unable to mount IFN response because of genetic ablation of the signaling receptors, are susceptible to PPRV. Different doses of PPRV (1, 10^2, 10^3 and 10^4 PFU) were i.p inoculated into IFNR KO mice and the disease progression was monitored (Fig 2A). We first measured the survival of PPRV infected animals up to eight dpi. All the infected animals succumbed to the infection albeit survival duration was dependent on the initial inoculum (Fig 2B). Accordingly, animals infected with the high dose died earlier as compared to those infected with the lower dose of PPRV (Fig 2B). We then measured other physiological parameters and body weights in the infected animals (Fig 2C). All the infected animals gradually lost their body weights, developed encephalitic lesions and became hypothermic (Fig 2C and data not shown). By 7dpi, all the animals succumbed to the infection irrespective of the doses of virus inoculum used (Fig 2C). In similar experiments, PPRV infected WT mice remained refractory to the PPRV induced disease as no clinical signs were observed even in those infected with the high infecting dose ($5x10^6$ PFU) (Fig 2B and C, S6B). The results, therefore, underscored the critical role of IFN signaling in providing an early defense against PPRV infection in mice.

PPRV infected mice expressed encephalitic lesions. We, therefore, measured the presence of PPRV antigens in the brain tissue sections by fluorescent microscopy using anti-PPRV (H) monoclonal antibodies. We also measured the replicating virus particles in brain tissue homogenates by performing plaque-forming assays. Fluorescent microscopic images of brain tissue sections from the infected animals revealed an abundance of viral antigens particularly when the animals were infected with the high doses of the virus inoculum (Fig 2D). A dose dependent increase in the PPRV loads was recorded in the homogenized brain tissues (Fig 2E). Accordingly, the replicating virus titers were 3.6 ± 0.3, 5.0 ± 0.4 and 6.4 ± 0.3 $\log_{10}$/g of brain tissues at the infecting dose of 1, 10^2 and 10^4 PFU, respectively (Fig 2E). We also collected different organs such as lungs, livers, hearts, brains and kidneys of mice infected with 1 or $1.5x10^6$ PFU of PPRV to measure the virus loads as well as to detect the presence of viral antigens (Fig 2F-H). The fluorescent microscopic images showed the presence of PPRV antigens in the tissue sections of liver, lung and heart of infected animals given $1.5x10^6$ PFU (Fig 2F). The virus titers in liver, lung and heart were 7.3 ± 1.0, 5.2 ± 0.5 and 4.9 ± 0.08 $\log_{10}$ PFU/g of tissue, respectively (Fig 2G). The virus load in the animals infected with a low dose of 1 PFU of PPRV were 4.3 ± 0.8, 5.8 ± 0.8, 6.0 ± 0.3, 6.1 ± 0.2 and 5.7 ± 0.8 PFU $\log_{10}$/g of tissue in heart, lungs, liver, spleen and kidneys, respectively (Fig 2H). Our results therefore suggested an active replication of PPRV in different organs of mice deficient in IFNs signaling.

IFNR KO mice were susceptible to PPRV infection even at a very low inoculum size (1PFU); we therefore investigated whether or not the infecting dose qualitatively influenced the disease. The brain tissue sections from animals infected with varying doses of PPRV were stained with H&E and the single cell suspensions

389 from brain tissues were analyzed by flow cytometry (Fig 2I). A high dose of PPRV
390 induced swelling of meninges in the infected brain tissues (Fig 2I, right panel).
391 Interestingly, the stained sections of brain tissues from animals infected with low
392 dose of PPRV (1PFU) showed greater leukocytic infiltration as compared to those
393 infected with the high dose (Fig 2I, left panel). We also analyzed the phenotype of
394 leukocytes from the single cell suspension of brain tissues by flow cytometry. The
395 leukocytes ($CD45^+$ cells) were analyzed for neutrophils ($CD11b^+Gr1^+$) and
396 macrophages ($CD11b^+F4/80^+$). Significantly higher frequencies of neutrophils were
397 present in the brain samples of PPRV infected mice as compared to the uninfected
398 controls (Fig 2J and K). The frequencies of macrophages also increased but the
399 results were not statistically different in control and infected mice (Fig 2L and M).
400 The increase in the frequencies of innate immune cells further supported the results
401 that the infected mice developed encephalitic lesions.

402 Many members of genus morbillivirus are neurovirulent and the PPRV
403 induced neurovirulence in naturally infected goat neonates was shown recently (21-
404 23). Therefore, the infectivity of IFNR KO mice by PPRV, their observed
405 neurovirulence as well as immune cells infiltration in infected tissues could suggest
406 that these mice could represent a better accessible model for deciphering molecular
407 and cellular mechanisms occurring during PPRV pathogenesis.

408 **Innate immune cells are permissive to PPRV infectivity**

409 We established the infectivity of IFNR KO mice and showed the
410 responsiveness of adaptive and innate immune cells. We then measured the immune
411 response in spleens of PPRV infected IFNR KO mice (Fig 3). The frequencies of
412 innate immune cells such as neutrophils ($CD11b^+Gr1^+$) increased by upto 10 fold in
413 PPRV infected mice as compared to controls (Fig 3A and B). Other innate immune

cells such as macrophages ($CD11b^+F4/80^+$) and DCs ($CD11b^+CD11c^+$) also showed a significant increase in PPRV infected mice in comparison to control but to a lesser extent as compared to those of neutrophils (Fig 3F, G, K and L). A rapid induction of innate immune cells after PPRV infection and the expression of encephalitic lesions in infected IFNR KO mice even at a low dose of the virus led us to explore the possibility of virus transport to CNS by such cells. We, therefore, measured the infectivity of innate immune cells by PPRV using intracellular staining for the viral proteins. Neutrophils ($Gr1^+$), macrophages ($F4/80^+$), and DCs ($CD11c^+$) from control and the infected animals were measured for the presence of PPRV heamaglutinin (H) and nucleocapsid (N) proteins using monoclonal antibodies (24). In morbilliviruses, N proteins are highly conserved and represent a major component of ribonucleoprotein complex while the H proteins help virus attach to the target cells. A significantly higher frequency of neutrophils isolated from PPRV infected mice showed the presence of H and N viral proteins (Fig 3C-E). Although PPRV proteins were also present in the macrophages and DCs of infected animals but the results were not statistically significant (Fig 3H-J and M-O). Therefore, neutrophils and perhaps other innate immune cells by virtue of their PPRV infectivity might contribute to the virus transport to different tissues.

Innate immune cells transport PPRV to central nervous system

We investigated whether or not innate immune cells help transport PPRV to CNS. PPRV infected innate immune cells were adoptively transferred in congenic mice followed by monitoring the disease progression in recipients (Fig 4A). Neutrophils, macrophages and dendritic cells were FACS sorted from WT congenic mice ($CD45.1^+$). The sorted cells were infected with PPRV and after extensive washings; these cells were transferred into sex matched IFNR KO mice ($CD45.2^+$)

(Fig 4A). We recovered enhanced frequencies of neutrophils ($CD45.1^+CD11b^+Gr1^+$, ~ 4%) and macrophages ($CD45.1^+CD11b^+F4/80^+$, ~ 2%) from brain tissues of recipients (Fig 4B and C). Moreover, the transferred PPRV-pulsed cells resulted in a patent infection in recipients with the progression of disease being similar to that observed in PPRV only injected animals (Fig 4D). This data suggested that infected innate immune cells particularly the neutrophils and macrophages could support virus replication and transport PPRV to different organs. We did not recover significantly higher frequencies of donor DCs ($CD45.1^+CD11b^+CD11c^+$) in the brain tissues of recipient mice but the disease severity was comparable in all the recipients (Fig 4B-D). Several factors could explain these results such as the inability of transferred DCs to directly home to brain tissues or their inefficient proliferation. Nonetheless, such cells might have transferred the virus to other inflammatory cells, which then could have transported it to brain tissues and elsewhere. The observed increased leukocytic infiltration in the brain tissues supported this notion (data not shown). Further analysis of different innate immune cells pulsed with PPRV demonstrated their infectivity as PPRV antigens could be detected in such cells by flow cytometry (Fig 4E and F). These results indicated that the virus could either be internalized by innate immune cells or be associated to surfaces and such cells could transport PPRV to distant sites such as the CNS.

PPRV induces lung pathologies in IFNR KO animals infected with intranasal route

PPRV causes respiratory disease in infected small ruminants and the infection spreads among animals in the herd due to their closer association, we therefore investigated its pathogenesis in mice infected via intranasal route. IFNR KO animals were infected with varying doses of PPRV and were analyzed for their survival, body

464 weights and other physiological parameters (Fig 5). The survival analysis of animals
465 showed a significant effect of inoculum sizes but all infected animals eventual
466 outcome in all the animals remained same as was observed in the i.p. infected mice
467 (Fig S2). Thus, animals infected with the lower dose (10^2PFU) succumbed to the
468 infection later and those infected with the higher doses (10^6PFU) died within 6 days.
469 For performing the cellular analysis at the tissue sites and lymphoid organs of
470 animals, additional groups of infected animals were sacrificed when approximately
471 20% of their body weights were lost (Fig 5A, S3-6). WT animals were infected with
472 a high dose (10^6 PFU/mouse) as all i.p infected animals with the higher inoculum
473 size survived (Fig 2B-C, data not shown). Infected WT animals reduced their body
474 weights transiently followed by their rapid recovery until the termination of the
475 experiments while the infected IFNR KO animals gradually reduced their body
476 weights at both the doses (10^4 PFU and 10^6 PFU) of PPRV (Fig 5B). The animals
477 were terminally anaesthetized at 6dpi for performing cellular analysis in collected
478 BALs, lungs, brain and lymphoid organs. Approximately two fold higher infiltration
479 level of leukocytes was observed in the BALs of WT animals as compared to the
480 IFNR KO animals suggesting for the immune reactivity against PPRV (Fig 5C). We
481 observed an enhanced infiltration of leukocytes in the BALs (~ 42% vs 30%) as well
482 as lung tissues (27% vs 19%) of IFNR KO animals infected with the low (10^2 PFU)
483 and high (10^4 PFU) dose of PPRV (Fig 5C and D). That the infiltrating leukocytes
484 could be involved in protection against the virus was indicated by their inverse ratios
485 observed in the lung tissues of two groups of PPRV infected animals (Fig 5C and D).
486 This could suggest that an efficient viral control could be achieved before a patent
487 lung infection is established and leukocytes are recruited. A minimal infiltration of
488 leukocytes was evident in the brain tissues of IFNR KO and WT animals infected via

intranasal route and the observed frequencies were similar in both the groups of mice (Fig 5E). We then phenotypically characterized different immune cells among the leukocyte populations in different organs. The relative abundance of macrophages ($CD11b^+F4/80^+$), neutrophils ($CD11b^+Gr1^+$), NK cells ($NK1.1^+$ cells), helper ($CD4^+$) and cytotoxic ($CD8^+$) T cells was measured in the non-lymphoid as well as lymphoid organs of infected WT and IFNR KO mice (Fig 5F-Z). Upto a five fold reduction in the frequencies of macrophages and neutrophils were observed in the BALs, lung tissues, brain, mediastinal LNs and spleens of infected WT animals as compared to those in IFNR KO mice (Fig 5G, H, K, L, P, Q, R, W and X). The frequencies of NK cells were similar in BALs but decreased in the lung and spleen of the PPRV infected WT animals as compared to those in IFNR KO mice (Fig 5I, M and Y). The increased frequencies of both $CD4^+$ and $CD8^+$ T cells in BALs and lung tissues of PPRV infected WT mice in comparison to those of the IFNR KO mice were observed (Fig 5J and N). BALs and mediastinal LNs of infected IFNR KO animals injected with different doses strikingly had more frequencies of neutrophils at a lower dose as compared to those at high dose (Fig 5H and R). Such a trend was not observed in lung tissues, brain and spleen samples of the infected animals (Fig 5L, P and X). The inverse correlation with PPRV inoculum size and the recruitment of macrophages was not observed in lungs, brain and spleens of IFNR KO animals infected (Fig 5G, K O and W). Enhanced frequencies of NK cells but a reduction in the frequencies of neutrophils and macrophages were observed for both BAL and lung tissues of WT mice (Fig 5G – I and K-M). Similarly, the frequencies of both $CD4^+$ and $CD8^+$ T cells increased in the spleens, BALs and lung tissues of PPRV infected WT mice that efficiently controlled PPRV infection (Fig 5F, J and N). These results suggested for the anti-PPRV activity of NK cells and T cells.

We further explored whether or not PPRV infection induces the activation of T cells. A significant proportion of $CD4^+$ T cells displayed an activation profile ($CD62L^{lo}CXCR3^+$) in WT animals but the frequencies of such cells were up to three fold higher in the IFNR KO animals (Fig 5S and T, S5). However, the frequencies of activated $CD62L^{lo}CXCR3^+$ $CD8^+$ T cells was ~2 fold lower in WT animals as compared to those in IFN RKO mice (Fig 5U and V, S5). Innate immune cells such as the NK cells in WT animals could help achieve an efficient viral control but such mechanisms might require the activity of IFNs as abundant replicating viral particles were present in the IFNR KO animals. Furthermore, the antigen presenting cells stimulated both $CD4^+$ and $CD8^+$ T cells but such cells were compromised in their function owing to their lack of type I IFN responsiveness.

Taken together, the analysis of cellular infiltration suggested for the role of neutrophils in promoting PPRV pathogenesis while NK cells and T cells playing protective roles.

IFN responsive $CD8^+$ T cells delay mortality in PPRV infected IFNR KO mice

We established the susceptibility of IFNR KO mice to PPRV, the potential spread of PPRV by infected innate immune cells and expansion of innate immune cells as well as T cells in PPRV infected WT mice that controlled the virus well (Fig S6B). We then explored whether WT T cells could either protect infected IFNR KO animals or reduce the severity of PPRV infection. FACS sorted $CD4^+$ and $CD8^+$ T cells from WT mice were transferred into IFNR KO animals. Such cells were allowed to expand for 40 days in recipients, which were then infected with PPRV (Fig S7A). In comparison to infected controls that gradually lost their body weight, $CD8^+$ T cell recipients showed a significantly reduced body weights until their termination at 6dpi (Fig S7B). WT $CD4^+$ T cell recipient mice and those received bone marrow cells did

not shown alteration in the rates or the kinetics of body weight loss (Fig S7B, data not shown). The activation status of $CD8^+$ and $CD4^+$ T cells of control and T cell recipient mice revealed more frequencies of $CD4^+$ and $CD8^+$ T cells expressing high levels of CD44 when WT $CD8^+$ T cells were transferred (Fig S7C-F, data not shown). These results suggest anti-viral activity of WT $CD8^+$ T cells.

We then measured whether or not previously PPRV-primed WT $CD8^+$ T cells confer protection to the PPRV infected IFNR KO mice. $5x10^6$ of FACS sorted WT $CD8^+$ T cells from naïve or the mice previously infected with PPRV were transferred before infecting IFNR KO mice with PPRV (Fig 6A). The survival analysis showed a significant advantage conferred to the infected IFNR KO mice by transferred naïve or primed $CD8^+$ T cells in delaying mortality (Fig 6B). Such effects occurred in a dose dependent manner with animals receiving five fold lower $CD8^+$ T cells succumbed to the infection early (Fig S7 and data not shown). Separate groups of PPRV infected $CD8^+$ T cell recipients were measured for a change in their body weights and cellular analysis on 7dpi (Fig S8 and S9). $CD8^+$ T cell recipients showed significantly reduced body weights by 6dpi (Fig 6C). Cellular analysis showed that approximately 50% of $CD45^+$ cells were present in the BAL of PPRV infected animals and the frequencies decreased to 30% in $CD8^+$ T cells recipients (Fig 6D). Similarly in the lung tissues of infected animals the frequencies of $CD45^+$ cells reduced from 25% to 15% in $CD8^+$ T cells recipients (Fig 6E). However, such effects were prominently observed in the group receiving $CD8^+$ T cells from previously PPRV-infected animals. Neutrophils levels increased in the BALs of $CD8^+$ T cell recipients IFNR KO mice by ~1.5 fold but the macrophages and NK cells decreased by ~ 10% (Fig 6F(a)-F(c)). In the lungs tissues, no significant differences in the cellular infiltrations were observed but for an increase in macrophages in $CD8^+$ T cell recipients (Fig 6G). The cellular analysis in

564 the MLN and spleen samples of infected animals revealed a reduction in the
565 frequencies of innate immune cells such as neutrophils and macrophages but more
566 $CD4^+$ and $CD8^+$ T cells were observed in WT $CD8^+$ T cell recipient mice (Fig 6J and
567 H). Phenotypic characterization of $CD4^+$ and $CD8^+$ T cells in control and WT $CD8^+$ T
568 cell recipient PPRV infected IFNR KO mice showed a reduced expression of the
569 activation molecule CXCR3 and as well as a lymph node retention molecule CD62L
570 (Fig 6I). However in the spleen of WT $CD8^+$ T cell recipient mice the expression of
571 CXCR3 was increased but that of CD62L reduced by both $CD4^+$ and $CD8^+$ T cells
572 (Fig 6K). These results might mean suggest for the retention of $CD8^+$ T cells in the
573 LNs of infected animals probably due to more chemokines build up and a less
574 efficient gradient generation for such chemokines to facilitate their exit and viral
575 control at the infection sites (25). A detailed analysis is currently underway.

576 We observed an aberrant activation profile of T cells in PPRV infected mice,
577 but a crucial role of functionally competent $CD8^+$ T cells was evident in mitigating
578 PPRV pathogenesis.

579 **Identification of immunogenic $CD8^+$ T cell epitopes of PPRV *in silico***

580 We identified immunogenic epitopes of PPRV that could induce specific
581 $CD8^+$ T cells response in mice. All the structural proteins (heamagglutinin, matrix,
582 nucleocapsid and fusion proteins) of PPRV were analyzed for predicting $H\text{-}2K^b$
583 restricted epitopes using IEDB database. We focused our analysis on the structural
584 proteins because such proteins are critical for the viral assembly and its envelope
585 formation (24). Peptides with low percentile ranks and the IC_{50} value of <200nM
586 were selected (Table S1). Out of the list generated, top 12 best ranking peptides (three
587 from each protein) were chosen for synthesis and further analysis (Fig 7A). The
588 peptides included in analysis were IVVRRTAGV, VAFNILVTL, FMYLFLLGV

589 (matrix protein), FSAGAYPLL, ASFILTIKF, SSITTRSRL (Nucleocapsid protein),
590 VILDRERLV, IEHIFESPL, IGLVRDFGL (hemagglutinin protein) and
591 (AILTFLFLL, VAILTFLFL, SGGDFLAIL (fusion protein). The peptides were
592 subjected to *in silico* analysis. Molecular docking is one of the most frequently used
593 methods to predict the conformation of small-molecule ligands. Docking of selected
594 peptides from different proteins of PPRV against H-2K^{b} was performed and the
595 models were analyzed using Chimera tool. The energy parameters of the best fitting
596 structures among PPRV peptides were determined (Table S2 and S3). The best
597 docking results were provided by PPRV peptides FMYLFLLGV and FSAGAYPLL
598 with H-2K^{b}. FMYLFLLGV peptide even yielded better docking scores then the
599 reference peptide FAPGNYPAL (SEV-9) of Sendai E virus (Fig 7B and D and Table
600 S2). Further analyses revealed phenylalanine residues at position 1 and 5 in
601 FMYLFLLGV peptide as the probable anchors. Similarly, for FSAGAYPLL peptide
602 phenylalanine at position 1 and proline at position 7 were predicted to be the most
603 probable anchors. Docking of peptides was also performed with class MHC molecule
604 of goat (CLA1) (Fig 7C and F, S10 and Table S3). CLA-I and H-2K^{b} superposed near
605 perfectly at an RMSD value of 1.5A (Fig 7E). The predicted peptides showed a
606 similar trend of docking with CLA-1 molecule. The anchor residues as well as the
607 docking scores of FMYLFLLGV and FSAGAYPLL peptides scored better in these
608 analyses (Fig 7E-F). Interestingly, all the epitopes displayed better docking with
609 CLA-1 than with H-2K^{b} indicating their immunogenicity in generating anti-viral
610 response against PPRV infection in the natural host, goats (Fig 7F). A total of 12
611 peptides were predicted that could potentially be immunogenic in mice as well as in
612 the natural host of PPRV goats.

Assessing class I MHC stabilization potential of predicted PPRV epitopes using acellular and cellular assays

We tested all top performing peptides for their class I MHC stabilization potential using acellular and cellular assays. SIINFEKL, an Ova derived peptide with known immunogenicity for H-2K^b, was used as a positive control. In order to measure the MHC stabilizing potential of predicted epitopes, we performed ELISA. The heterotrimeric complex consisting of a photocleavable ligand, β2 microglobulin and H-2K^b was immobilized to solid phase by plate-coated streptavidin. UV displaced conditional ligand and its replacement with the testing peptide yields a positive reaction that can be detected by anti-β2 microglobulin antibody (16). Fold change values as compared to those obtained for SIINFEKL peptide for each of the PPRV derivative peptides are shown in Fig 8A. Accordingly, FSAGAYPLL, IGLVRDFGL, AILTFLFLL, SSITTRSRL, IVVRRTAGV, IEHIFESPL, VAFNILVTL, and VILDRERLV displayed higher values as compared to other peptides (Fig 8A).

The peptides were also analysed for their class I MHC stabilizing activities using transporter associated with antigen processing and presentation (TAP) deficient RMA/S cells. Such cells express fewer molecules of class I MHCs on surface but the exogenously added immunogenic peptides help stabilize their expression (26). Different concentrations PPRV peptides were added to serum starved RMA/S cells (Fig 8B-D). Out of 12 peptides, four peptides FMYLFLLGV (matrix protein), FSAGAYPLL (nucleocapsid protein), IGLVRDFGL (hemagglutinin protein) and AILTFLFLL (fusion protein) showed higher affinity for H-2K^b molecule and induced more cells to express H-2K^b (Fig 8B-D). The results were dependent on the concentrations of the peptides used (Fig 8B-D). Similar results were obtained when the mean fluorescence intensity (MFI) values were measured for the expression of H-

638 2K^b by each peptide (data not shown). Log EC_{50} values for AILTFLFLL,
639 FSAGAYPLL, IGLVRDFGL and FMYLFLLGV peptides were 2.098, 1.469, 1.228
640 and 1.268 µg/ml, respectively (Fig 8D).

641 **Immunogenicity of PPRV peptides in PPRV infected or immunized mice**

642 We measured response of CD8$^+$ T cells in PPRV infected and immunized
643 mice. As C57BL/6 mice were refractory to PPRV infection, we used a high dose of
644 PPRV (5x10^6 PFU) PPRV for infection. After 7 days, a boosting dose was given and
645 the analysis was done in blood samples three days later by measuring the numbers
646 and frequencies of class I MHC tetramer (H-2K^b-p(PPRV)-tetramer). Our results
647 showed significantly more numbers of antigen-specific CD8$^+$ T cells against
648 AILTFLFLL, FSAGAYPLL and IGLVRDFGL peptides of PPRV as compared to
649 those induced against FMYLFLLGV (Fig 9A-C). Tetramer positive CD8$^+$ T cell
650 count was also high for FSAGAYPLL, IGLVRDFGL peptides in animals immunized
651 with the cocktail of four peptides (Fig. 9D-E). The functionality of PPRV specific
652 CD8$^+$ T is currently being investigated.

653 Our results suggest an induction of CD8$^+$ T cell response against predicted
654 PPRV epitopes. Therefore, our results also suggest that immunization with peptides
655 could represent a potential subunit vaccination approach for PPRV to investigate
656 properties of CD8$^+$ T cells during PPRV infection in mice.

657

658

Discussion

With ramped up efforts to eradicate PPRV by intensive vaccination programs, it has become imperative to develop an accessible laboratory animal model to better understand its pathogenesis and more importantly the immune correlates of protection against the virus. Such investigation could enhance prospects of devising an alternative vaccine strategies should a need arise. We undertook this study to develop a laboratory mouse model to elucidate PPRV pathogenesis, the role of innate immune cells and cytotoxic T cells in its control. We demonstrated the susceptibility of IFNR KO mice to PPRV infection. The infected animals succumbed to PPRV infection irrespective of the dose of inoculum and route of infection. The replicating viruses as well as the derivative antigens were present abundantly in most of the critical organs of infected mice. Neutrophils and macrophages likely served as the Trojan horse to transport virus to the CNS to cause encephalitis while $CD8^+$ T cells in addition to NK cells were protective in PPRV infected mice. We also discovered immunogenic epitopes of PPRV and enumerated virus-specific $CD8^+$ T cells in infected and immunized mice C57BL/6 mice using an array of MHC tetramers. Our results showed the infectivity of adult mice that can serve as a laboratory animal model for investigating PPRV pathogenesis and further decipher protective role of $CD8^+$ T cells.

PPRV, a member of morbilivirus genus of paramyxoviridae family, incurs significant losses to animal husbandry sector in endemic areas (27). Therefore, intensive vaccination programs are being adopted in many countries to eradicate the virus. A laboratory mouse model would be useful not only to better understand the contribution of cellular and molecular mediators in the viral of pathogenesis but also to test the efficacy of anti-virals. One such class of host-derived molecules includes type I IFNs that have potent anti-viral effects. We observed distinct expression pattern

of type I IFNs induced by PPRV stimulated innate immune cells depending on the dose of infecting virus, and the intrinsic properties of responding cells (RAW macrophages versus bone marrow derived primary macrophages). These results could suggest for a diversification in the function of type I IFNs. Such a phenomenon is well documented for the activity of type I and type III IFNs that was shown to be largely attributed to the expression pattern of their cognate receptors (28). While the receptors for type I IFNs (IFNAR1 and IFNAR2) are ubiquitously present on most cells, type III IFNRs (IFNL complex) are predominantly present in epithelial cells and only a subset of innate immune cells such as neutrophils (27, 29). A dichotomy is also known with the activity of type I IFNs i.e., IFNα and IFNβ(30). Furthermore, a specific inhibition of IFNβsignaling by antibodies converted the course of a persistent viral infection with LCMV clone 13 into an infection that could be efficiently controlled in the acute phase (31). Therefore, further analysis to decipher the relative roles of different species of type I IFNs in the protection against PPRV would be valuable.

In WT animals the activity of NK cells might control PPRV infection sufficiently and $CD4^+$ and $CD8^+$ T cells playing a subsidiary antiviral role (Fig 5). We observed efficient infiltration of NK cells in the BAL and lung tissues but the animals eventually succumbed to the infection (Fig 5I and M). These results suggested a critical role of IFN signaling in the NK cells mediated control of PPRV and the killing activity of such cells alone might not suffice to achieve viral control. The expansion and the migration of T cells particularly of $CD4^+$ T cells in PPRV infected WT mice in comparisons to those in the IFNR KO mice could suggest for a critical role played by IFN signaling in the efficient activation or the migration of such cells which can then help efficient priming of $CD8^+$ T cells. That the $CD4^+$ T

709 cell responses precede $CD8^+$ T cells was shown earlier (32). Earlier reports also
710 suggested that an inefficient JAK/STAT signaling in $CD8^+$ T cells that occur
711 following type I IFN ligation with their cognate receptors enhances the propensity of
712 such cells to undergo apoptosis by host factors such as the glucocorticoids. Multiple
713 studies have shown that microbial infections can actively engage hypothalamic
714 pituitary adrenal (HPA) axis to induce glucocorticoids able to induce the apoptosis of
715 $CD8^+$ T cells (17). Whether or not PPR infection predominantly activate HPA axis is
716 not known currently. That $CD8^+$ T cells are involved in anti-PPRV defense
717 mechanisms was shown by the adoptive transfer of WT $CD8^+$ T cells, isolated from
718 previously infected mice that resolved the infection (Fig 6).

719 With limited data available for PPRV cell and tissue tropism, its replication
720 was demonstrated in the lymphoid organs (6). The known receptor for PPRV are
721 SLAM family proteins (33). Our results demonstrated that the cells of innate immune
722 origin expanded upon PPRV infection in IFNR KO mice were susceptible to the viral
723 infection. Surprisingly innate immune cells such as neutrophils and macrophages
724 were potentially able to transfer virus to distal locations (Fig 3 and 4). The innate
725 immune cells express SLAM receptors abundantly and therefore their susceptibility to
726 PPRV infection could involve these receptors (33). The identification of a particular
727 receptor in the susceptibility of mice has not been explored and constitutes part of our
728 ongoing investigations. It would be interesting to explore whether PPRV replicates in
729 the innate immune cells of sheep and goats. If indeed such cells exhibit susceptibility
730 to PPRV, it might necessitate revisiting vaccination strategies to help achieve a
731 complete viral eradication. Neurovirulence and neuropathology induced by PPRV are
732 recently reported in goat kids and newly born BALB/c mice as well as CD1d
733 knockout mice, the latter induce inefficient NK cells responses (22, 23). However the

734 susceptibility of IFNR KO mice to PPRV was not shown earlier. Our observations
735 could be more relevant for some herds that might have mutations in one or more
736 components of signaling pathways involving type I IFNs. Animals and humans with
737 signaling defects in pathways leading to type I IFN production are exceedingly
738 susceptible to viral infections (21, 34). We used a vaccine strain of PPRV that
739 induced a hundred percent mortality in IFNR KO mice and no apparent disease in WT
740 C57BL/6 mice. Whether or not the virulent strain of PPRV can induce the disease and
741 potent CTL response in WT mice is currently being investigated in our laboratory.

742 An initial encounter of host with viruses elicit type I IFN response, but for a
743 long term protection the optimal activity of $CD8^+$ T cells is crucial in virus clearance
744 (17, 35). This necessitates identifying class I epitopes that can be used to quantify and
745 assess functionality of such cells (11). Moreover, designing a vaccine against an
746 intracellular pathogen also requires information about immunogenic epitopes that can
747 also serve as subunit vaccine candidates. Screening of peptides of an antigen is best
748 done by *in silico* analysis as invariably a large number of linear amino acid sequences
749 need to be probed. The utility of class I MHC tetramers in staining antigen-specific
750 $CD8^+$ T cells and discovering epitopes in a throughput manner is unmatched but has
751 not been adequately put to use particularly for animal pathogens (18, 36). The
752 prediction of peptide is necessary for diagnosis, formulating vaccines as well as for
753 analyzing the functionality of cells (11, 18, 37). We discovered at least four
754 immunogenic epitopes from structural proteins of PPRV using *in silico, ex vivo* and *in*
755 *vivo* approaches. That the immunization of mice with a cocktail of peptides induced
756 PPRV specific $CD8^+$ T cells constitute first such example for PPRV. Furthermore
757 such an approach provides impetus to subunit vaccine development. Our ongoing

758 investigations would help decipher pathways in virus specific $CD8^+$ T cells that could

759 help provide protection during acute as well as memory response.

760 **References**

761 1. Diallo A, Minet C, Le Goff C, Berhe G, Albina E, Libeau G, Barrett T. 2007.
762 The threat of peste des petits ruminants: progress in vaccine development for
763 disease control. Vaccine 25:5591–5597.
764 2. Singh RK, Balamurugan V, Bhanuprakash V, Sen A, Saravanan P, Yadav MP.
765 2009. Possible control and eradication of peste des petits ruminants from India:
766 technical aspects. Vet Ital 45:449–462.
767 3. Kumar P, Tripathi BN, Sharma AK, Kumar R, Sreenivasa BP, Singh RP, Dhar
768 P, Bandyopadhyay SK. 2004. Pathological and immunohistochemical study of
769 experimental peste des petits ruminants virus infection in goats. J Vet Med Ser
770 B 51:153–159.
771 4. Mahapatra M, Parida S, Egziabher BG, Diallo A, Barrett T. 2003. Sequence
772 analysis of the phosphoprotein gene of peste des petits ruminants (PPR) virus:
773 editing of the gene transcript. Virus Res 96:85–98.
774 5. Baron MD, Parida S, Oura CAL. 2011. Peste des petits ruminants: a suitable
775 candidate for eradication? Vet Rec 169:16–21.
776 6. Truong, T. Boshra, H. Embury-Hyatt, C. Nfon, C. Gerdts, V, Tikoo, S. Babiuk,
777 LA. Kara, P. Chetty, T. Mather, A. Wallace, DB. Babiuk S. 2014. Peste des
778 Petits Ruminants Virus Tissue Tropism and Pathogenesis in Sheep and Goats
779 following Experimental Infection. PLoS One 9:e87145.
780 7. Berhe, G. Minet, C. Le Goff, C. Barrett, T. Ngangnou, A. Grillet, C. Libeau, G.
781 Fleming, M. Black, DN. Diallo A. 2003. Development of a dual recombinant
782 vaccine to protect small ruminants against peste-des-petits-ruminants virus and
783 capripoxvirus infections. J Virol 77:1571–7.
784 8. Reed L, Muench H. 1938. A simple method of estimating fifty percent end

785 points. Am J Epidemiol 27:493–497.

786 9. Wang C, Yu X, Cao Q, Wang Y, Zheng G, Tan TK, Zhao H, Zhao Y, Wang Y,
787 Harris DCH. 2013. Characterization of murine macrophages from bone
788 marrow, spleen and peritoneum. BMC Immunol 14:6.

789 10. Moutaftsi M, Peters B, Pasquetto V, Tscharke DC, Sidney J, Bui H-H, Grey H,
790 Sette A. 2006. A consensus epitope prediction approach identifies the breadth
791 of murine TCD8+-cell responses to vaccinia virus. Nat Biotechnol 24:817–819.

792 11. Calis JJA, Maybeno M, Greenbaum JA, Weiskopf D, De Silva AD, Sette A,
793 Keşmir C, Peters B. 2013. Properties of MHC class I presented peptides that
794 enhance immunogenicity. PLoS Comput Biol 9.

795 12. Peters B, Bui H-H, Frankild S, Nielsen M, Lundegaard C, Kostem E, Basch D,
796 Lamberth K, Harndahl M, Fleri W. 2006. A community resource
797 benchmarking predictions of peptide binding to MHC-I molecules. PLoS
798 Comput Biol 2.

799 13. Remmert M, Biegert A, Hauser A, Söding J. 2012. HHblits: lightning-fast
800 iterative protein sequence searching by HMM-HMM alignment. Nat Methods
801 9:173.

802 14. Pettersen EF, Goddard TD, Huang CC, Couch GS, Greenblatt DM, Meng EC,
803 Ferrin TE. 2004. UCSF Chimera—a visualization system for exploratory
804 research and analysis. J Comput Chem 25:1605–1612.

805 15. Sehrawat S, Kirak O, Koenig P-A, Isaacson MK, Marques S, Bozkurt G, Simas
806 JP, Jaenisch R, Ploegh HL. 2012. CD8(+) T cells from mice transnuclear for a
807 TCR that recognizes a single H-2K(b)-restricted MHV68 epitope derived from
808 gB-ORF8 help control infection. Cell Rep 1:461–71.

809 16. Chew SL, Or MY, Chang CXL, Gehring AJ, Bertoletti A, Grotenbreg GM.

2011. Stability screening of arrays of major histocompatibility complexes on combinatorially encoded flow cytometry beads. J Biol Chem 286:28466–28475.

17. Kumar, D. Sehrawat S. 2019. Divergent Effects of a Transient Corticosteroid Therapy on Virus-Specific Quiescent and Effector CD8+ T Cells. Front Immunol 10:1521.

18. Rodenko B, Toebes M, Hadrup SR, Van Esch WJE, Molenaar AM, Schumacher TNM, Ovaa H. 2006. Generation of peptide–MHC class I complexes through UV-mediated ligand exchange. Nat Protoc 1:1120.

19. Freshney RI. 1987. Culture of animal cells: a manual of basic technique. New York: Alan R. Liss. Inc 1:177.

20. Kaur M, Kumar D, Butty V, Singh S, Esteban A, Fink GR, Ploegh HL, Sehrawat, S. 2018. Galectin-3 regulates gamma-herpesvirus specific CD8 T cell immunity. iScience 9, 101-119.

21. Rouse BT, Sehrawat S. 2010. Immunity and immunopathology to viruses: what decides the outcome? Nat Rev Immunol 10:514–526.

22. Galbraith SE, McQuaid S, Hamill L, Pullen L, Barrett T, Cosby SL. 2002. Rinderpest and peste des petits ruminants viruses exhibit neurovirulence in mice. J Neurovirol 8:45–52.

23. Sahoo M, Dinesh M, Thakor JC, Baloni S, Saxena S, Shrivastava S, Dhama K, Singh K, Singh R. 2020. Neuropathology mediated through caspase dependent extrinsic pathway in goat kids naturally infected with PPRV. Microb Pathog 140J vi:103949.

24. Saravanan, S. Singh, RP. Balamurugan, P. Saravanan, S. Sen, Sahay, B. Sarkar, J . Singh R. 2007. Production and Characterization of Neutralizing Monoclonal

835 Antibodies Against Haemagglutinin Protein of peste des petits ruminants (PPR)
836 Vaccine Virus. J Appl Anim Res 32:207–210.
837 25. Lund JM, Hsing L, Pham TT, Rudensky AY. 2008. Coordination of early
838 protective immunity to viral infection by regulatory T cells.
839 30;320(5880):1220-4.
840 26. Van Kaer, L. Ashton-Rickardt, P.G. Ploegh, H.L., Tonegawa S. 1992. TAP1
841 mutant mice are deficient in antigen presentation, surface class I molecules,
842 and CD4-8+ T cells. Cell 71:1205–1214.
843 27. Kumar N, Barua S, Riyesh T, Tripathi BN. 2017. Advances in peste des petits
844 ruminants vaccines. Vet Microbiol 206:91–101.
845 28. Galani IE, Triantafyllia V, Eleminiadou E-E, Koltsida O, Stavropoulos A,
846 Manioudaki M, Thanos D, Doyle SE, Kotenko S V, Thanopoulou K. 2017.
847 Interferon-λ mediates non-redundant front-line antiviral protection against
848 influenza virus infection without compromising host fitness. Immunity 46:875–
849 890.
850 29. Crotta, S. Davidson, S. Mahlakoiv, T. Desmet, CJ. Buckwalter, MR. Albert,
851 ML. Staeheli, P. Wack A. 2013. Type I and Type III Interferons Drive
852 Redundant Amplification Loops to Induce a Transcriptional Signature in
853 Influenza-Infected Airway Epithelia. PLoS Pathog 9:e1003773.
854 30. Wang, Y. Swiecki, M. Cella, M. Alber, G. Schreiber, RD. Gilfillan, S. Colonna
855 M. 2012. Timing and magnitude of type I interferon responses by distinct
856 sensors impact CD8 T cell exhaustion and chronic viral infection. Cell Host
857 Microbe 11:631–42.
858 31. Ng CT, Sullivan BM, Teijaro JR, Lee AM, Welch M, Rice S, Sheehan KC,
859 Schreiber RD, Oldstone M. 2015. Blockade of interferon Beta, but not

interferon alpha, signaling controls persistent viral infection. Cell Host Microbe 17:653–61.

32. Nakanishi Y, Lu B, Gerard C, Iwasaki A. 2009 CTL mobilization to virus-infected tissue requires CD4+ T cell help. Nature 26; 462(7272): 510–513.

33. Veillette A. 2006. Immune regulation by SLAM family receptors and SAP-related adaptors. Nat Rev Immunol 6:56–66.

34. Sehrawat S, Kumar D, Rouse BT. 2018. Herpesviruses: Harmonious Pathogens but Relevant Cofactors in Other Diseases? Front Cell Infect Microbiol 8:177.

35. Ahmed R, Kaech SM. 2001. Memory CD8+ T cell differentiation: initial antigen encounter triggers a developmental program in naïve cells. Nat Immunol 2:415–422.

36. Flynn KJ, Belz GT, Altman JD, Ahmed R, Woodland DL, Doherty PC. 1998. Virus-specific CD8+ T cells in primary and secondary influenza pneumonia. Immunity 8:683–691.

37. Rammensee H-G, Bachmann J, Emmerich NPN, Bachor OA, Stevanović S. 1999. SYFPEITHI: database for MHC ligands and peptide motifs. Immunogenetics 50:213–219.

879 **Figure legends**

880 **Figure 1. PPRV pulsed murine macrophages mount a rapid IFN response.**
881 Murine macrophages (RAW macrophages and primary bone marrow derived
882 macrophages) were pulsed with PPRV at low (1:1) and high (1:10) multiplicity of
883 infections (MOI) to measure IFNα, IFNβ and IFNγ response. The PPRV exposed
884 cells were collected at different times to isolate total RNA. cDNA synthesized was
885 measured for the expression of different IFNs by RT-qPCR. A-C. Fold change in the
886 expression of IFNα, β and γ is shown by bar diagrams at 15min, 30min, 1hr and 6hr.
887 D-F. BMDMs similarly analyzed for the expression of IFNα, β and γ at indicated
888 time points. Bar diagrams show fold change in the expression of IFNs. The
889 experiments were repeated six times. One way ANOVA test was used for
890 determining the statistical significance and p values are represented as following; $p < 0.05$ *, $p < 0.01$ **, $p < 0.001$***.
892 **Figure 2. IFNR KO mice are susceptible to PPRV infection.** A. The schematic of
893 experiments is shown. IFNR KO mice were i.p. infected with indicated doses of
894 PPRV and the survival analysis (B) and percentage change in body weight of mice
895 (C) from each group is shown. The level of statistical significance was determined by
896 Gehan-Breslow-Wilcoxon test and one-way ANOVA, respectively. Each data point
897 in the graph represents the average percent change in body weight at the indicated
898 dpi. Control animals were not infected with PPRV. D. Fluorescent microscopic
899 images show the presence of PPRV antigens in brain tissues of the infected IFNR
900 KO mice as detected by anti-PPRV (H) mAbs. E. Bar diagrams show PPRV titres as
901 represented by log10 PFU/g of tissue when measured by plaque forming assays using
902 brain tissues of i.p., infected IFNR KO mice administered with varying doses. F-G.
903 IFNR KO mice were i.p. infected with $1.5x10^6$ PFU of PPRV and different organs

were collected 4dpi to measure the presence of viral antigens (F) and replicating virus (G) in different organs. F. Fluorescent microscopic images show the presence of virus antigens in brain tissues of PPRV infected IFNR KO mice as detected by anti-PPRV (H) protein mAbs. G. Virus titers as represented by log10 PFU/g of tissue in heart, lung and liver is shown. Data represents the mean ± SD of three replicates of tissue samples. H. Virus titers as represented by log10 PFU/g of tissue are shown in different organs of IFNR KO mice infected with 1PFU of PPRV. I. Histopathological changes in virus infected brain sections are shown. The experiments were repeated three times with similar results. B-I. One way ANOVA test was used for determining the statistical significance values and are represented as following; $p < 0.05$ *, $p < 0.01$ **, $p < 0.001$***. J-M. Innate immune cells were analyzed in the brain tissues of PPRV infected IFNR KO mice. The single cell suspensions prepared from brain samples were stained with neutrophils ($CD11b^+Gr1^+$) and macrophages ($CD11b^+F4/80^+$). J. Representative FACS plots show the frequencies of $CD11b^+Gr1^+$ cells in control and PPRV infected mice. K. Bar diagrams show the cumulative data. L. Representative FACS plots show the frequencies of $CD11b^+F4/80^+$ cells in control and PPRV infected mice. M. Bar diagrams show the cumulative data. The experiments were repeated two times. Student t test were used form determining the significance levels in control and infected groups. $p < 0.05$ *, $p < 0.01$ **, $p < 0.001$ ***.

Figure 3. Determining PPRV infectivity of innate immune cells in IFNR KO mice. IFNR KO mice were i.p infected with 100PFU of PPRV and the expansion as well infectivity of innate immune cells was measured in spleen. A. Representative FACS plots show the frequencies of $Gr1^+$ cells among live cell gate in control and PPRV infected mice. B. Bar diagrams show cumulative data for the frequencies of

929 $Gr1^+$ cells in control and PPRV infected mice. C-E. Intracellular staining was
930 performed as described in the material and methods sections to measure the presence
931 of PPRV antigens in $Gr1^+$ cells using anti-PPRV (H) and anti-PPRV (N) protein
932 antibodies. C. Representative overlaid histograms show the frequency of PPRV
933 $(H)^+Gr1^+$ cells. D. Representative histograms show the percentage of PPRV
934 $(N)^+Gr1^+$ cells. E. Bar diagrams show cumulative data as percent positive $Gr1^+$PPRV
935 $(H)^+$ and PPRV $(N)^+$ cells. F. Representative FACS plots show the frequencies of
936 $F4/80^+$ cells among live cell gate in control and PPRV infected mice. G. Bar
937 diagrams show cumulative data for the frequencies of $F4/80^+$ cells in control and
938 PPRV infected mice. H-J. Intracellular staining was performed as described in the
939 materials and method section to measure the presence of PPRV antigens in $Gr1^+$ cells
940 using anti-PPRV H protein and anti-PPRV-N protein mAbs. H. Representative
941 overlaid histograms show the frequency of PPRV $(H)^+F4/80^+$ cells. I. Representative
942 histograms showing the percentage of PPRV $(N)^+F4/80^+$ cells. J. Bar diagrams show
943 the percentage of $F4/80^+$ cells expressing PPRV (H) and PPRV (N) proteins. K.
944 Representative FACS plots show the frequencies of $CD11c^+$ cells among live cell
945 gate in control and PPRV infected mice. L. Bar diagrams show cumulative data for
946 the frequencies of $CD11c^+$ cells in control and PPRV infected mice. M-O.
947 Intracellular staining was performed as described in the material and methods
948 sections to measure the presence of PPRV antigens in $CD11c^+$ cells using anti-PPRV
949 H protein and anti-PPRV-N protein antibodies. M. Representative overlaid
950 histograms show the frequency of PPRV $(H)^+CD11c^+$ cells. N. Representative
951 histograms show the percentage of PPRV $(N)^+CD11c^+$ cells. O. Bar diagrams show
952 the percentage of $F4/80^+$ cells expressing PPRV (H) and PPRV (N) proteins. The
953 experiments were repeated two times with four animals in each group. Different

954 groups were analyzed by two-way ANOVA using Sidak's multiple comparison test.
955 Statistical significance values are represented as following; $p < 0.05$ *, $p < 0.01$ **,
956 $p < 0.001$***.

957 **Figure 4. Innate immune cells serve as the carrier of PPRV to brain tissues.**
958 FACS sorted neutrophils, macrophages and dendritic cells from $CD45.1^{+}$ C57BL/6
959 mice were pulsed with PPRV and after washing transferred into $CD45.2^{+}$ IFNR KO
960 mice. At 4dpi, brain tissue staining was done with CD45.1 and CD45.2 markers. A.
961 Representative FACS plots depict the frequencies of donor cells in processed brain
962 tissue suspensions. B. Bar diagrams shown the cumulative frequencies of frequencies
963 expanded donor cells recovered from brain suspensions. For each group of recipients
964 three animals were used and the experiments were performed two times. C. FACS
965 sorted macrophages ($F4/80^{+ve}$), neutrophils ($Gr1^{+ve}$) and dendritic cells ($CD11c^{+ve}$)
966 from $CD45.1^{+}$ C57BL/6 mice were pulsed with PPRV for 1hr and transferred in
967 IFNR KO mice. The recipients were monitored for their body weights and morbidity.
968 D-E. FACS sorted macrophages ($F4/80^{+ve}$), neutrophils ($Gr1^{+ve}$) and dendritic cells
969 ($CD11c^{+ve}$) from $CD45.1^{+}$ C57BL/6 mice were pulsed with PPRV for 1hr. After
970 washings, cells were stained to determine the presence of surface or intracellular
971 viral antigens. Representative FACS plots show PPRV $(H)^{+ve}$ cells for each cell type.
972 For gating FACS plots, fluorescent minus one (FMO) parameter were used. E. Bar
973 diagrams show cumulative data for $PPRV^{+ve}$ cells. The experiments were repeated
974 two more times. One way ANOVA or Student t test were done for determining the
975 statistical significance values and are represented as following; $p < 0.05$ *, $p < 0.01$
976 **, $p < 0.001$***.

977 **Figure 5. IFNR KO mice infected with PPRV develop lung pathologies and**
978 **mount innate as well as adaptive immune responses.** A. IFNR KO and WT

C57BL/6 mice were infected with varying doses of PPRV via intranasal route and animals were analyzed for their survival, change in body weights. The level of statistical significance was determined by Gehan-Breslow-Wilcoxon test and one-way ANOVA, respectively. Terminally anaesthetized animals were analyzed for measuring the cellular infiltration in BAL, lungs and lymphoid organs at 7dpi. The FACS plots for gating strategy and representative plots from different groups of animals are shown in supplementary Fig S3-6. B. Percent change in body weights of WT and IFNR KO mice infected with PPRV is shown. C-E. The frequencies of leukocytes ($CD45^+$ cells) are shown in the BAL (C), lungs (D) and brain tissues (E) of infected WT and IFNR KO mice. F. Bar diagrams show the percentage of $CD4^+$ and $CD8^+$ T cells in the spleens of infected animals. G-J. Frequencies of macrophages ($CD11b^+F4/80^+$) (G), neutrophils ($CD11b^+Gr1^+$) (H), NK cells ($NK1.1^+$) (I) and T cells (J) are shown in the BAL of infected animals by bar diagrams. K-N. Frequencies of macrophages ($CD11b^+F4/80^+$) (K), neutrophils ($CD11b^+Gr1^+$) (L), NK cells ($NK1.1^+$) (M) and T cells (N) are shown in the lungs of infected animals by bar diagrams. O-P. Frequencies of macrophages ($CD11b^+F4/80^+$) (O) and neutrophils ($CD11b^+Gr1^+$) (P) are shown in the lungs of infected animals by bar diagrams. Q-V. Frequencies of macrophages ($CD11b^+F4/80^+$) (Q), neutrophils ($CD11b^+Gr1^+$) (R) and the phenotypic characterization $CD4^+$ T cells (S and T) and $CD8^+$ T cells (U-V) for the indicated markers are shown in the MLN of infected animals by bar diagrams. W-Z. Frequencies of macrophages ($CD11b^+F4/80^+$) (W) and neutrophils ($CD11b^+Gr1^+$) (X) and NK cells (Y) are shown in the spleen of infected animals by bar diagrams. Z. Activation profile of splenic $CD4^+$ T cells is shown by bar diagram. The experiments were repeated three times. The data was analyzed by two-way ANOVA was

performed for determining the statistical significance values. The levels of significance are represented as following; $p < 0.05$ *, $p < 0.01$ **, $p < 0.001$ ***.

Figure 6. WT CD8$^+$ T cells delay mortality in PPRV infected IFNR KO mice. A schematic of the experiments is shown. 5x10^6 of CD8$^+$ T cells from naïve or previously PPRV infected WT mice were transferred into IFNR KO mice. Next day, the recipient animals were infected with PPRV (10^{4}PFU). The disease progression, survival and cellular analysis of immune cells were performed. B. The survival in different groups of animals is shown. The results were analyzed by Gehan-Breslow-Wilcoxon test. C. Percent change in body weight of mice from each group is shown. The level of statistical significance was determined by Two-way ANOVA . D-E. The frequencies of leukocytes (CD45$^+$ cells) in BAL (D) and lungs (E) of infected mice are shown by bar diagrams. F-G. The frequencies of macrophages (CD11b$^+$F4/80$^+$), neutrophils (CD11b$^+$Gr1$^+$), NK cells (NK1.1$^+$) and T cells (both CD4$^+$ and CD8$^+$ T cells) are shown in the BAL (F) and lungs (G) of infected animals by bar diagrams. H. The frequencies of macrophages (CD11b$^+$F4/80$^+$), neutrophils (CD11b$^+$Gr1$^+$), NK cells (NK1.1$^+$), T cells (CD4$^+$ and CD8$^+$ T cells) are shown in the MLNs of infected animals by bar diagrams. I. The phenotypic characterization CD4$^+$ T cells and CD8$^+$ T cells for the indicated markers are performed and the percent positive cells frequencies for the indicated markers are shown for MLN of infected animals by bar diagrams. J. The frequencies of macrophages (CD11b$^+$F4/80$^+$), neutrophils (CD11b$^+$Gr1$^+$), NK cells (NK1.1$^+$), T cells (CD4$^+$ and CD8$^+$ T cells) are shown in the MLNs of infected animals by bar diagrams. K. The phenotypic characterization CD4$^+$ T cells and CD8$^+$ T cells for the indicated markers were performed and the frequencies of percent positive cells for the indicated markers are shown for spleen of infected animals by bar diagrams. The experiments were performed three times.

1029 The data was analysed by two-way ANOVA for determining the statistical
1030 significance values and are represented as following; $p < 0.05$ *, $p < 0.01$ **, $p <$
1031 0.001 ***.

1032 **Figure 7. Molecular docking reveals docking of predicted peptides binding with**
1033 **H-2K^b and CLA-I.** A. High scoring peptides and their origin of PPRV protein are
1034 tabulated. B. The docking scores of each peptide with H-2K^b are shown. C. The
1035 docking scores of each peptide with goat class I MHC (CLA-1) are shown by bar
1036 diagrams. D. Selected peptides for further evaluation in *ex vivo* and *in vivo* assays
1037 with their predicted molecular docking scores are shown. E. H-2K^b and CLA-1 were
1038 superimposed at RMSD value of 1.5A. F. A comparative analysis of docking scores
1039 of H-2K^b and CLA-I for the predicited PPRV peptides is shown.

1040 **Figure 8. Immunogenicity of predicted peptides of PPRV was determined by *in***
1041 ***vitro* assays.** A. An ELISA was performed for measuring the stabilization of H-2K^b
1042 monomers by synthetic peptides predicted to be immunogenic. The bar diagrams
1043 show folds change values for H-2K^b positive cells for the respective peptides as
1044 compared to the control peptide. B. Representative overlay histograms for different
1045 concentrations (50µg/ml, 25µg/ml, 12.5µg/ml and 6.25µg/ml) of indicated peptides
1046 show their ability to stabilize surface MHC molecules. The values represent the
1047 percent positive cells at different concentrations of peptides. C. Bar diagrams show
1048 percent H-2K^b positive cells for different concentrations of the indicated peptides. D.
1049 Line graph shows log EC_{50} values for different peptides for stabilizing H-2K^b in
1050 pulsed RMA/s cells. Student t test were performed for determining the statistical
1051 significance values and are represented as following; $p < 0.05$ *, $p < 0.01$ **, $p <$
1052 0.001 ***.

Figure 9. PPRV infected and PPRV-peptide immunized WT C57BL/6 mice expand virus-specific CD8$^+$ T cells. A-C. WT C57BL/6 mice (n=5) were i.p. infected with 5x10^6 PFU of PPRV at an interval of 7 days. The analysis of the expanded cells was performed three days later by measuring the frequencies PPRV-specific CD8$^+$ T cells by staining with arrays of tetramers. A. Representative FACS plots shown the frequencies of class I MHC tetramer positive cells for the indicated peptides. B. Frequencies of PPRV-specific CD8$^+$ T cells are shown by bar diagrams. C. The number of cells/million of PBMCs is shown by bar diagrams. D-E. C57BL/6 mice (n=4) were immunized either with the cocktail of peptide (AILTFLFLL, FMYLFLLGV, FSAGAYPLL and IGLVRDFGL) each with 5µg/mouse in complete Freund's adjuvant via subcutaneous route. After two weeks, a second injection of the same concentration was administered as an emulsion with incomplete Freund's adjuvant. Three days later the frequencies of peptide specific CD8$^+$ T cells were measured by tetramer staining of PBMCs. D. Representative FACS plots show the frequencies of PPRV-specific CD8$^+$ T cells. E. The number of cells/million of PBMCs is shown by bar diagrams. The experiments were repeated two times and the statistical significance was measured by Student t test. $p < 0.05$ *, $p < 0.01$ **.

Figure 1

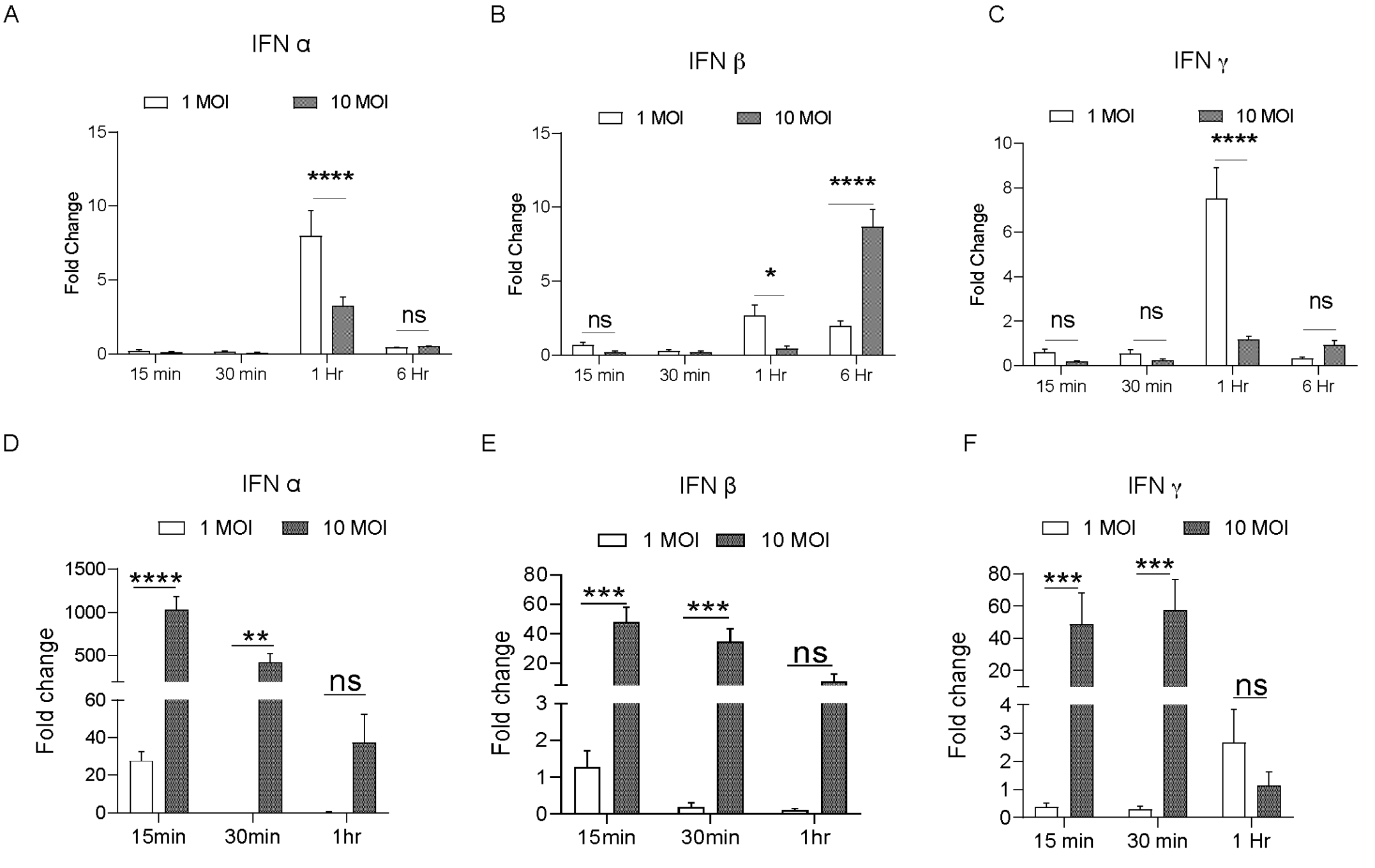
A
IFN α
1 MOI
10 MOI
Fold Change
15
10
5
0
****
ns
15 min
30 min
1 Hr
6 Hr
B
IFN β
1 MOI
10 MOI
Fold Change
15
10
5
0
ns
*
****
15 min
30 min
1 Hr
6 Hr
C
IFN γ
1 MOI
10 MOI
Fold Change
10
8
6
4
2
0
ns
ns
****
ns
15 min
30 min
1 Hr
6 Hr
D
IFN α
1 MOI
10 MOI
Fold change
1500
1000
500
60
40
20
0
****
**
ns
15min
30min
1hr
E
IFN β
1 MOI
10 MOI
Fold change
80
60
40
20
3
2
1
0
***
***
ns
15min
30min
1hr
F
IFN γ
1 MOI
10 MOI
Fold change
80
60
40
20
4
3
2
1
0
***
***
ns
15 min
30 min
1 Hr

Figure 2

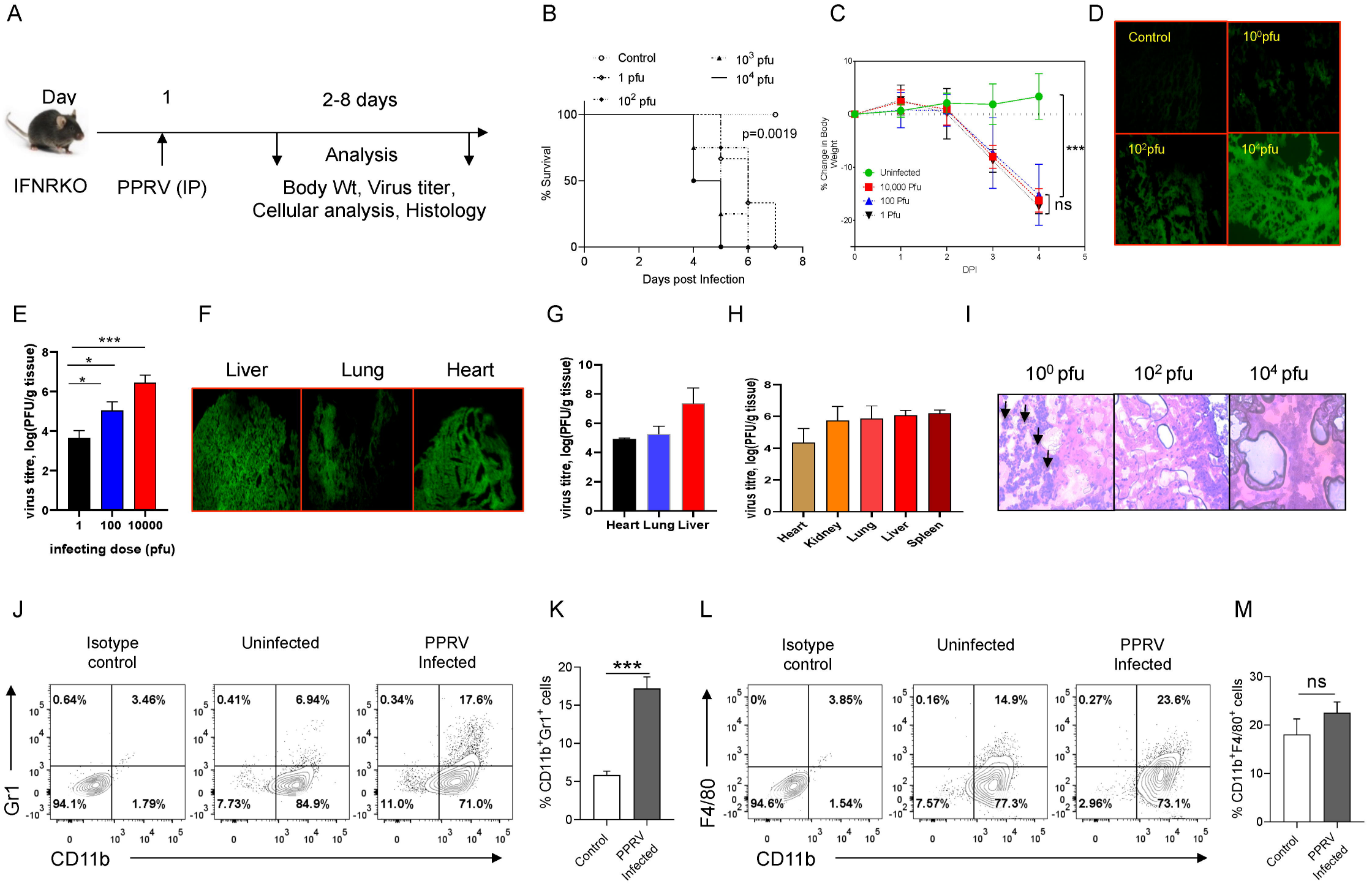
A
Day
1
2-8 days
IFNRKO
PPRV (IP)
Analysis
Body Wt, Virus titer,
Cellular analysis, Histology
B
Control
1 pfu
10^2 pfu
10^3 pfu
10^4 pfu
p=0.0019
% Survival
Days post Infection
C
% Change in Body Weight
Uninfected
10,000 Pfu
100 Pfu
1 Pfu
***
ns
DPI
D
Control
10^0pfu
10^2pfu
10^4pfu
E
virus titre, log(PFU/g tissue)
infecting dose (pfu)
1
100
10000
F
Liver
Lung
Heart
G
virus titre, log(PFU/g tissue)
Heart Lung Liver
H
virus titre, log(PFU/g tissue)
Heart
Kidney
Lung
Liver
Spleen
I
10^0 pfu
10^2 pfu
10^4 pfu
J
Isotype control
Uninfected
PPRV Infected
Gr1
CD11b
0.64%
3.46%
94.1%
1.79%
0.41%
6.94%
7.73%
84.9%
0.34%
17.6%
11.0%
71.0%
K
% CD11b+Gr1+ cells
***
Control
PPRV Infected
L
Isotype control
Uninfected
PPRV Infected
F4/80
CD11b
0%
3.85%
94.6%
1.54%
0.16%
14.9%
7.57%
77.3%
0.27%
23.6%
2.96%
73.1%
M
% CD11b+F4/80+ cells
ns
Control
PPRV Infected

Figure 3

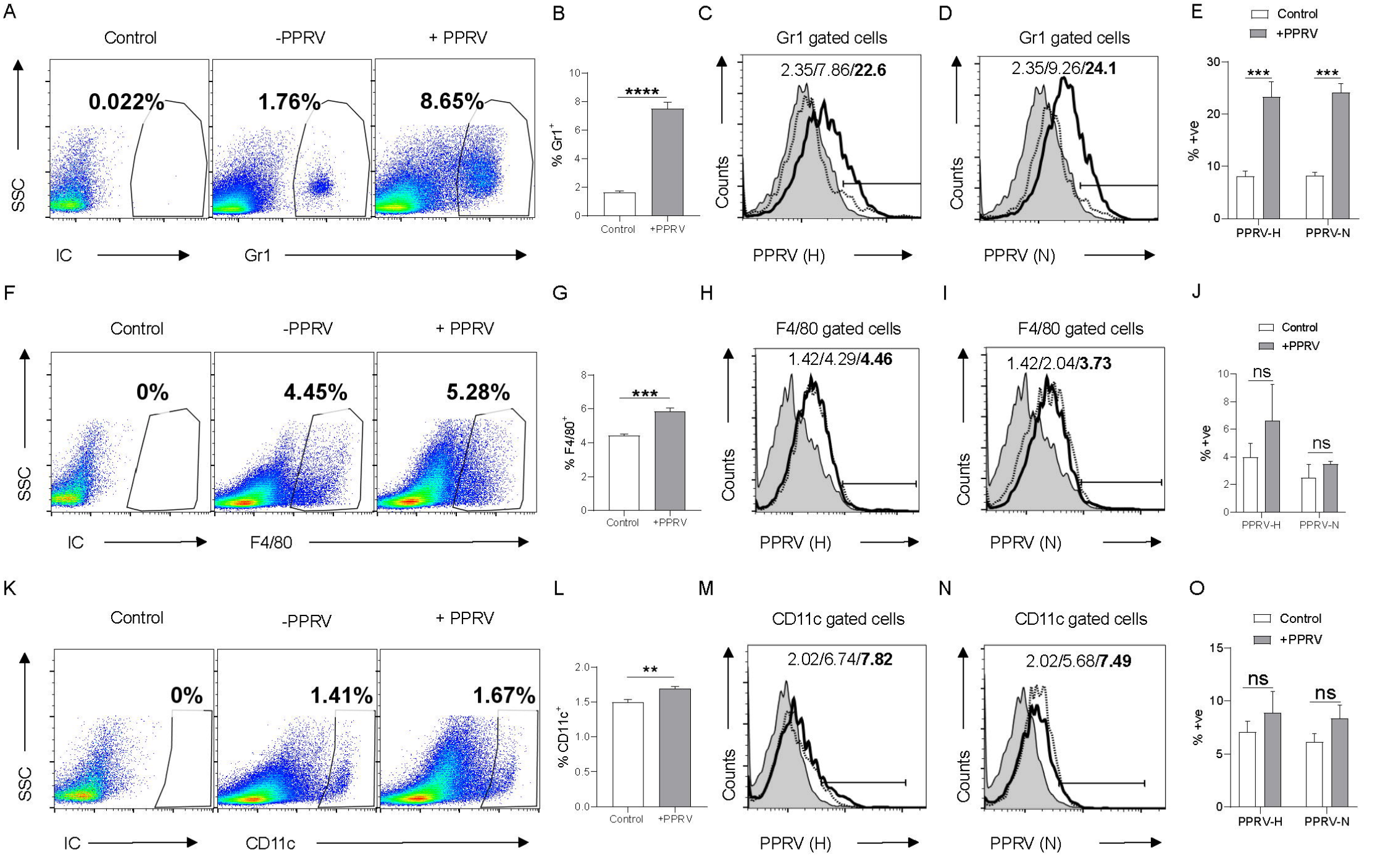
A
Control
-PPRV
+ PPRV
0.022%
1.76%
8.65%
SSC
IC
Gr1
B
% Gr1+
****
Control
+PPRV
C
Gr1 gated cells
2.35/7.86/22.6
Counts
PPRV (H)
D
Gr1 gated cells
2.35/9.26/24.1
Counts
PPRV (N)
E
Control
+PPRV
% +ve
***
***
PPRV-H
PPRV-N
F
Control
-PPRV
+ PPRV
0%
4.45%
5.28%
SSC
IC
F4/80
G
% F4/80+
***
Control
+PPRV
H
F4/80 gated cells
1.42/4.29/4.46
Counts
PPRV (H)
I
F4/80 gated cells
1.42/2.04/3.73
Counts
PPRV (N)
J
Control
+PPRV
% +ve
ns
ns
PPRV-H
PPRV-N
K
Control
-PPRV
+ PPRV
0%
1.41%
1.67%
SSC
IC
CD11c
L
% CD11c+
**
Control
+PPRV
M
CD11c gated cells
2.02/6.74/7.82
Counts
PPRV (H)
N
CD11c gated cells
2.02/5.68/7.49
Counts
PPRV (N)
O
Control
+PPRV
% +ve
ns
ns
PPRV-H
PPRV-N

Figure 4

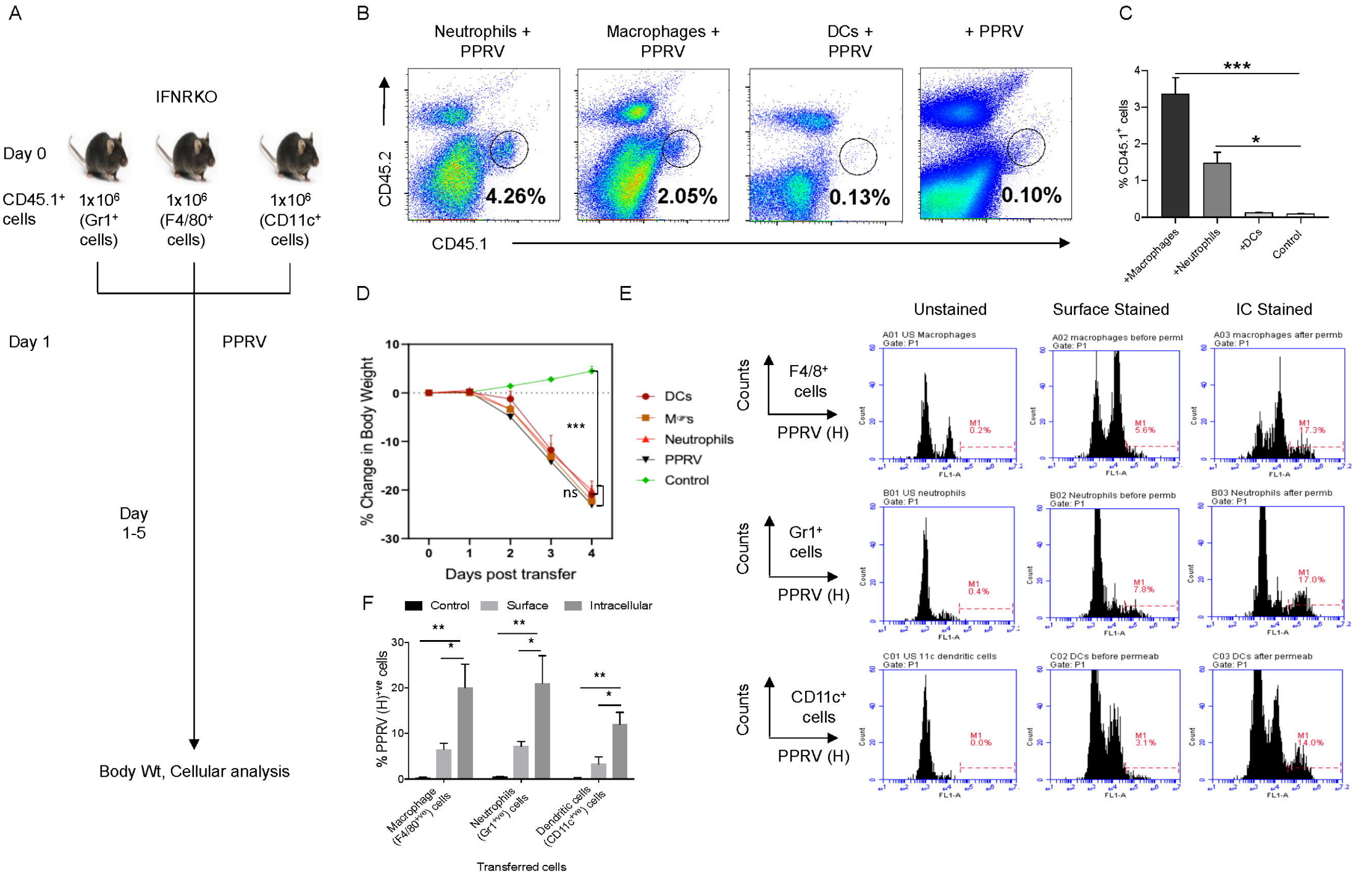
A
IFNRKO
Day 0
CD45.1+ cells
1x10^6 (Gr1+ cells)
1x10^6 (F4/80+ cells)
1x10^6 (CD11c+ cells)
Day 1
PPRV
Day 1-5
Body Wt, Cellular analysis
B
Neutrophils + PPRV
Macrophages + PPRV
DCs + PPRV
+ PPRV
CD45.2
CD45.1
4.26%
2.05%
0.13%
0.10%
C
% CD45.1+ cells
***
*
+Macrophages
+Neutrophils
+DCs
Control
D
% Change in Body Weight
Days post transfer
DCs
Mφs
Neutrophils
PPRV
Control
***
ns
E
Unstained
Surface Stained
IC Stained
Counts
F4/8+ cells
PPRV (H)
Gr1+ cells
CD11c+ cells
A01 US Macrophages Gate: P1
A02 macrophages before permi Gate: P1
A03 macrophages after permb Gate: P1
M1 0.2%
M1 5.6%
M1 17.3%
B01 US neutrophils Gate: P1
B02 Neutrophils before permb Gate: P1
B03 Neutrophils after permb Gate: P1
M1 0.4%
M1 7.8%
M1 17.0%
C01 US 11c dendritic cells Gate: P1
C02 DCs before permeab Gate: P1
C03 DCs after permeab Gate: P1
M1 0.0%
M1 3.1%
M1 14.0%
FL1-A
F
Control
Surface
Intracellular
% PPRV (H)+ve cells
Macrophage (F4/80+ve) cells
Neutrophils (Gr1+ve) cells
Dendritic cells (CD11c+ve) cells
Transferred cells

Figure 5

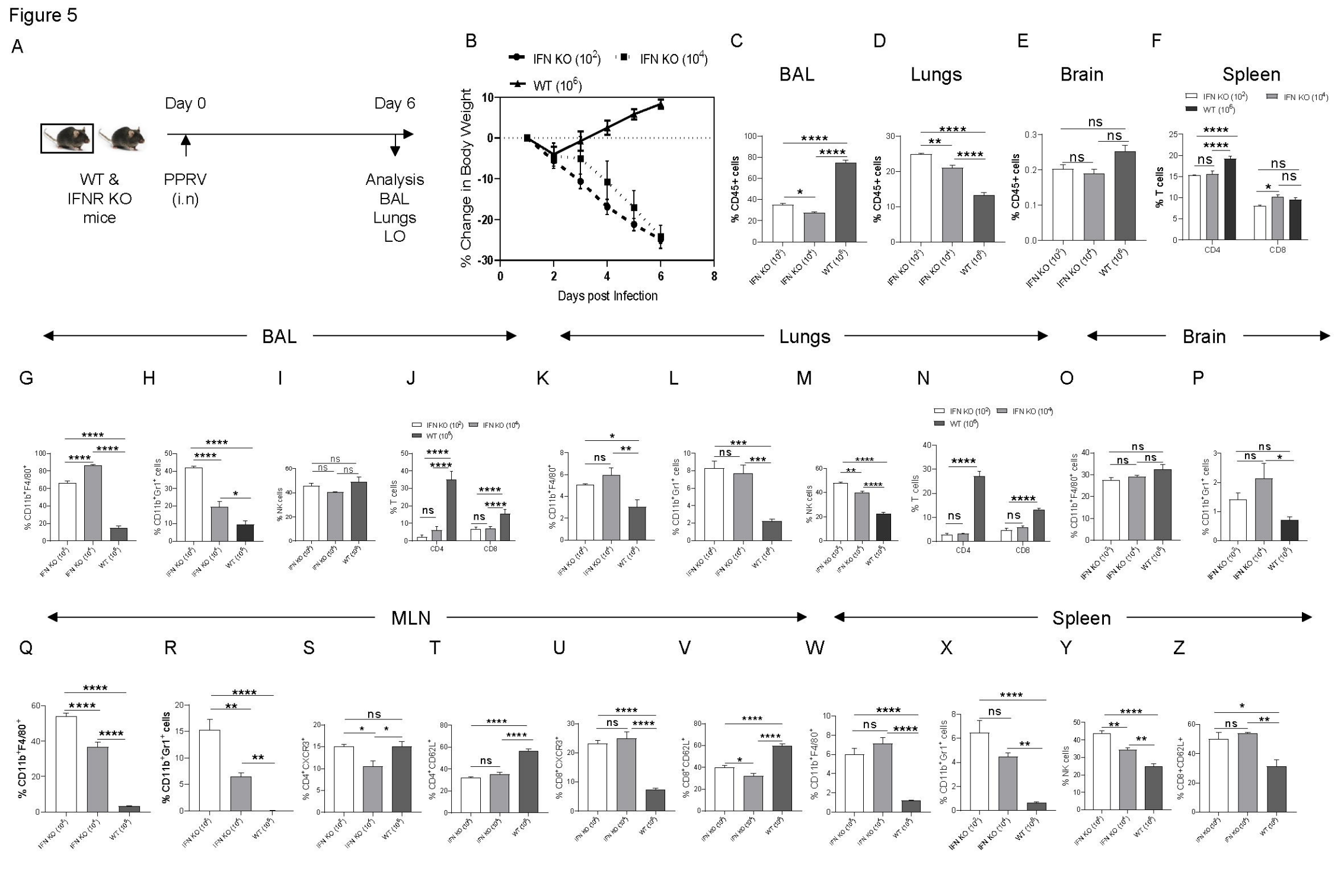
A
Day 0
Day 6
WT &
IFNR KO
mice
PPRV
(i.n)
Analysis
BAL
Lungs
LO
B
IFN KO (10²)
IFN KO (10⁴)
WT (10⁶)
% Change in Body Weight
Days post Infection
C
BAL
D
Lungs
E
Brain
F
Spleen
% CD45+ cells
% T cells
CD4
CD8
BAL
Lungs
Brain
G
H
I
J
K
L
M
N
O
P
% CD11b⁺F4/80⁺
% CD11b⁺Gr1⁺ cells
% NK cells
% T cells
MLN
Spleen
Q
R
S
T
U
V
W
X
Y
Z
% CD4⁺CXCR3⁺
% CD4⁺CD62L⁺
% CD8⁺CXCR3⁺
% CD8⁺CD62L⁺
% CD8+CD62L⁺

Figure 6

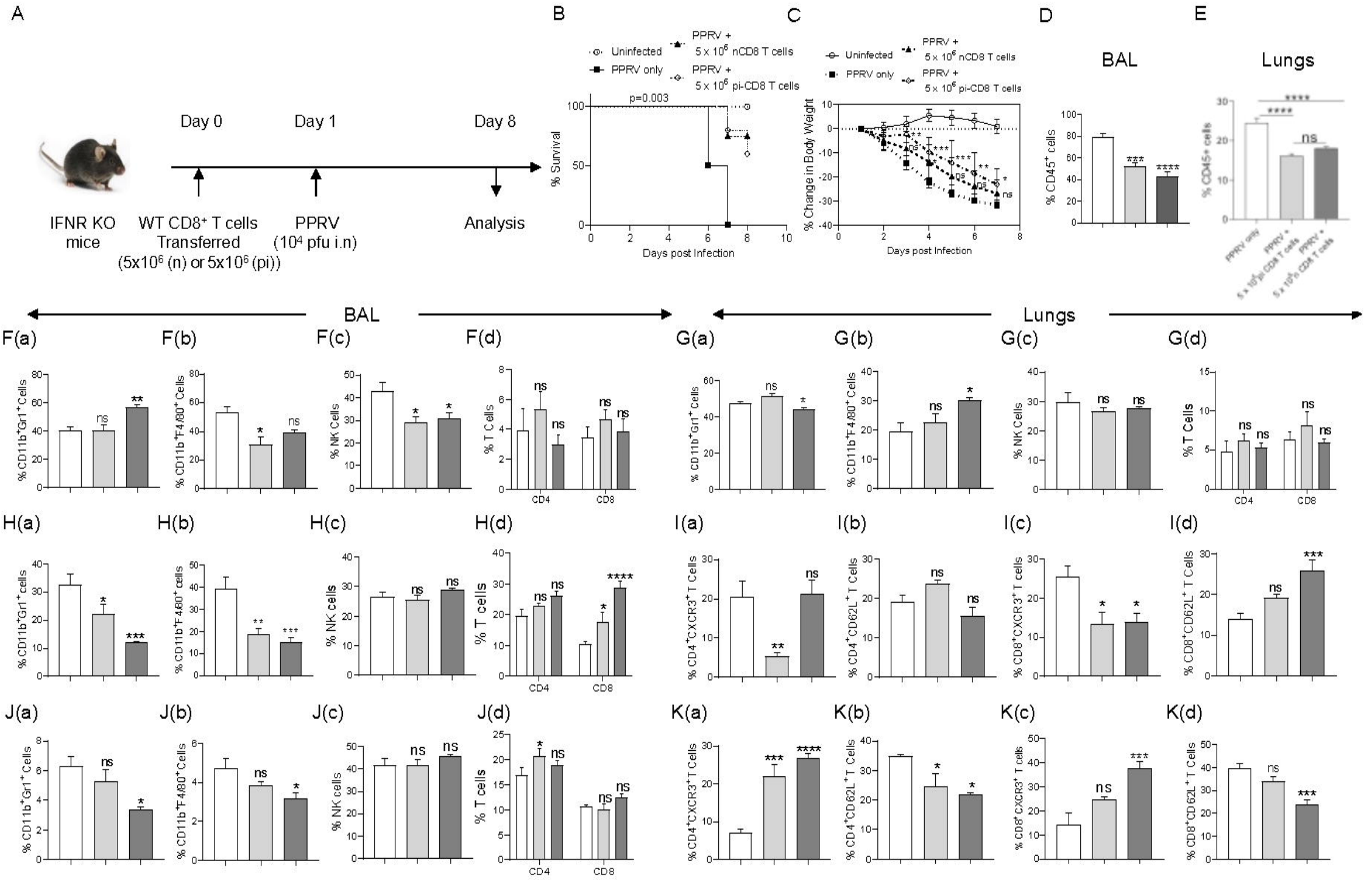
A
Day 0
Day 1
Day 8
IFNR KO mice
WT CD8+ T cells Transferred (5x10^6 (n) or 5x10^6 (pi))
PPRV (10^4 pfu i.n)
Analysis
B
Uninfected
PPRV only
PPRV + 5 x 10^6 nCD8 T cells
PPRV + 5 x 10^6 pi-CD8 T cells
p=0.003
% Survival
Days post Infection
C
% Change in Body Weight
Days post Infection
D
BAL
% CD45+ cells
E
Lungs
% CD45+ cells
BAL
Lungs
F(a)
% CD11b+Gr1+ Cells
F(b)
% CD11b+F4/80+ Cells
F(c)
% NK Cells
F(d)
% T Cells
CD4
CD8
G(a)
% CD11b+Gr1+ Cells
G(b)
% CD11b+F4/80+ Cells
G(c)
% NK Cells
G(d)
% T Cells
CD4
CD8
H(a)
% CD11b+Gr1+ cells
H(b)
% CD11b+F4/80+ cells
H(c)
% NK cells
H(d)
% T cells
CD4
CD8
I(a)
% CD4+CXCR3+ T Cells
I(b)
% CD4+CD62L+ T Cells
I(c)
% CD8+CXCR3+ T cells
I(d)
% CD8+CD62L+ T Cells
J(a)
% CD11b+Gr1+ Cells
J(b)
% CD11b+F4/80+ Cells
J(c)
% NK cells
J(d)
% T cells
CD4
CD8
K(a)
% CD4+CXCR3+ T Cells
K(b)
% CD4+CD62L+ T Cells
K(c)
% CD8+CXCR3+ T cells
K(d)
% CD8+CD62L+ T Cells

Figure 7

A

PPRV PROTEIN	H-2K^b
Fusion	AILTFLFLL VAILTFLFL SGGDFLAIL
Nucleocapsid	FSAGAYPLL ASFILTIKF SSITTRSRL
Hemagglutinin	VILDRERLV IEHIFESPL IGLVRDFGL
Matrix	IVVRRTAGV VAFNILVTL FMYLFLLGV

B

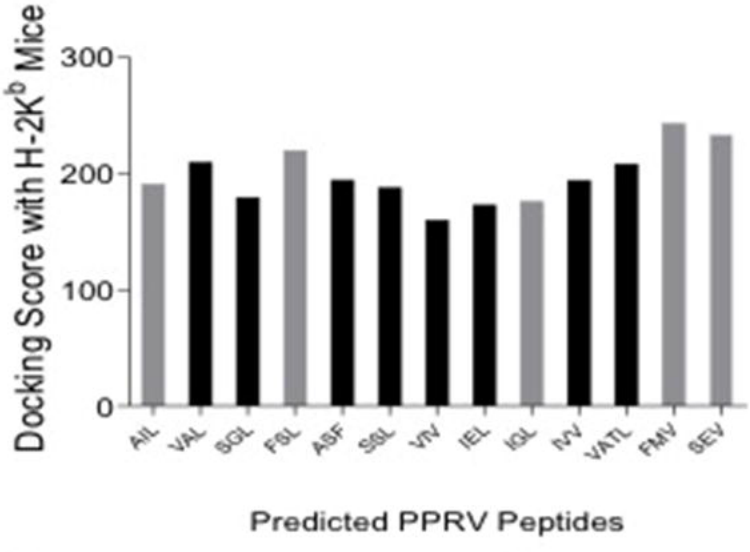

C

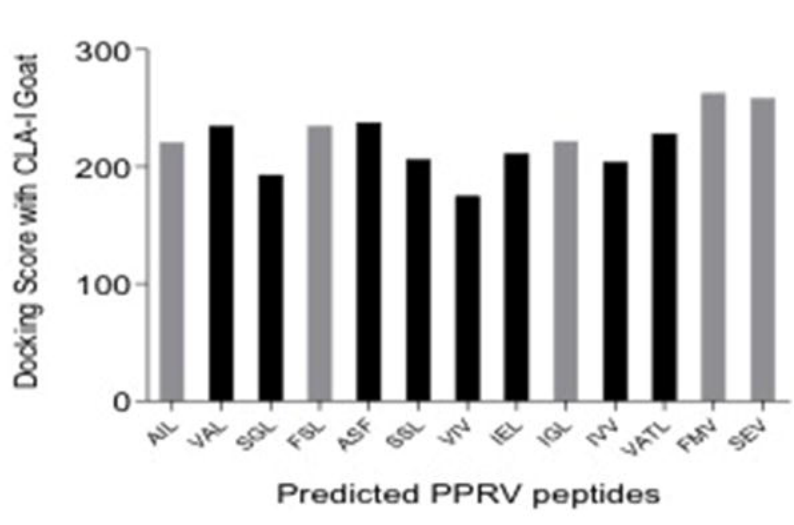

D

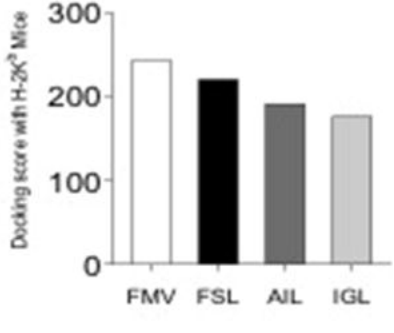

E

F

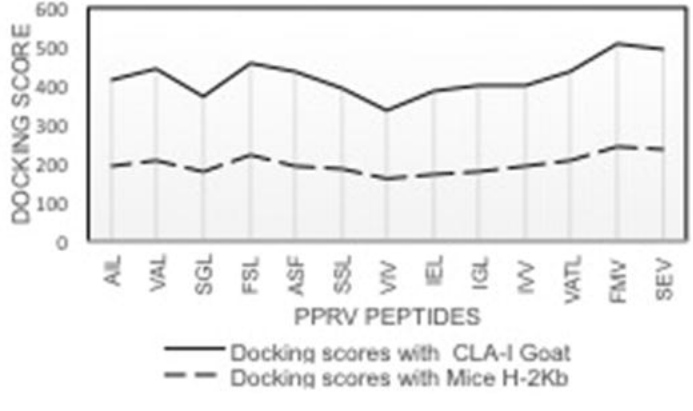

Figure 8

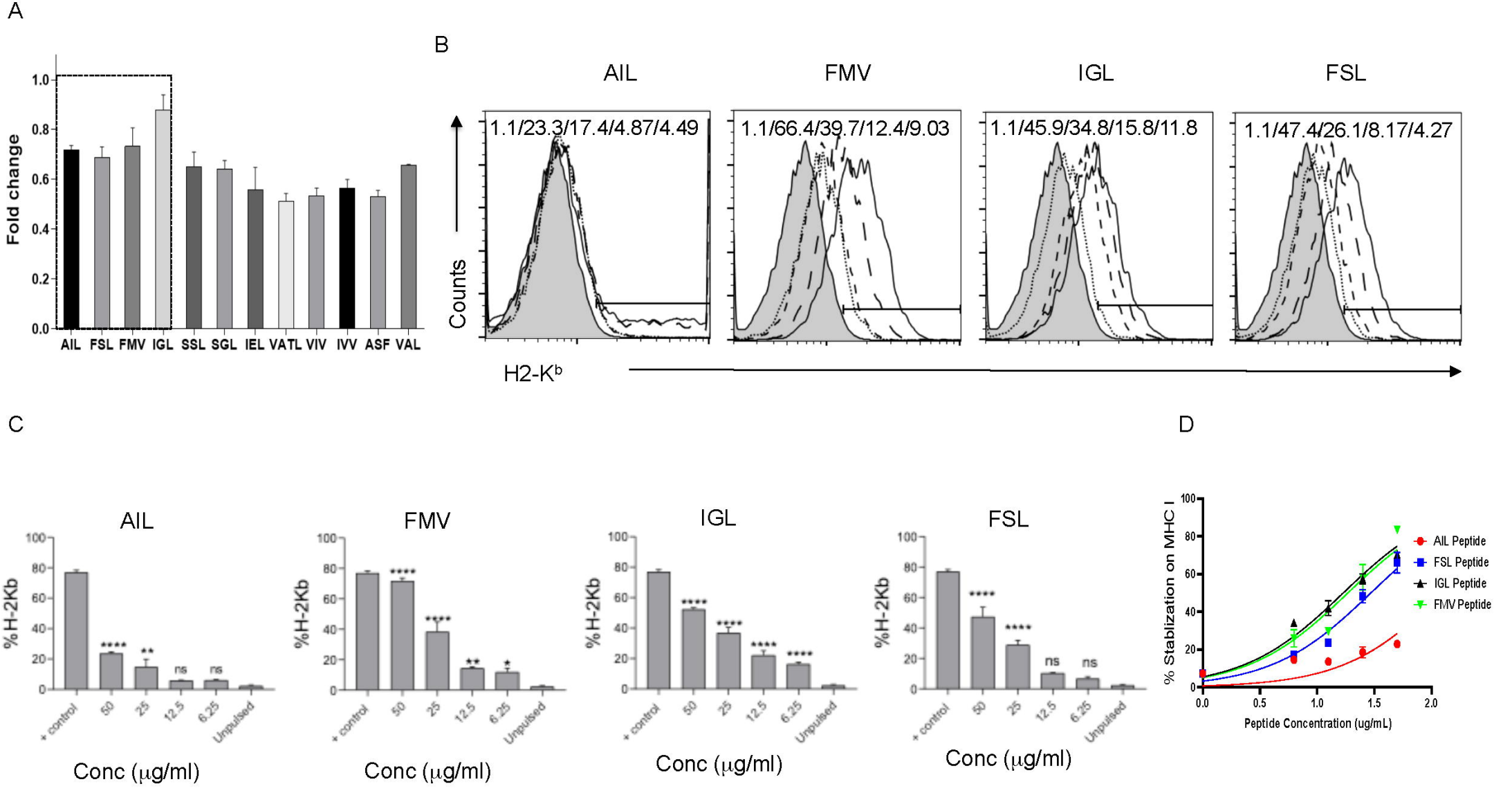
A
Fold change
1.0
0.8
0.6
0.4
0.2
0.0
AIL FSL FMV IGL SSL SGL IEL VATL VIV IVV ASF VAL
B
AIL
FMV
IGL
FSL
1.1/23.3/17.4/4.87/4.49
1.1/66.4/39.7/12.4/9.03
1.1/45.9/34.8/15.8/11.8
1.1/47.4/26.1/8.17/4.27
Counts
H2-Kb
C
AIL
FMV
IGL
FSL
%H-2Kb
+ control
50
25
12.5
6.25
Unpulsed
Conc (μg/ml)
D
% Stablization on MHC I
Peptide Concentration (ug/mL)
AIL Peptide
FSL Peptide
IGL Peptide
FMV Peptide

Figure 9

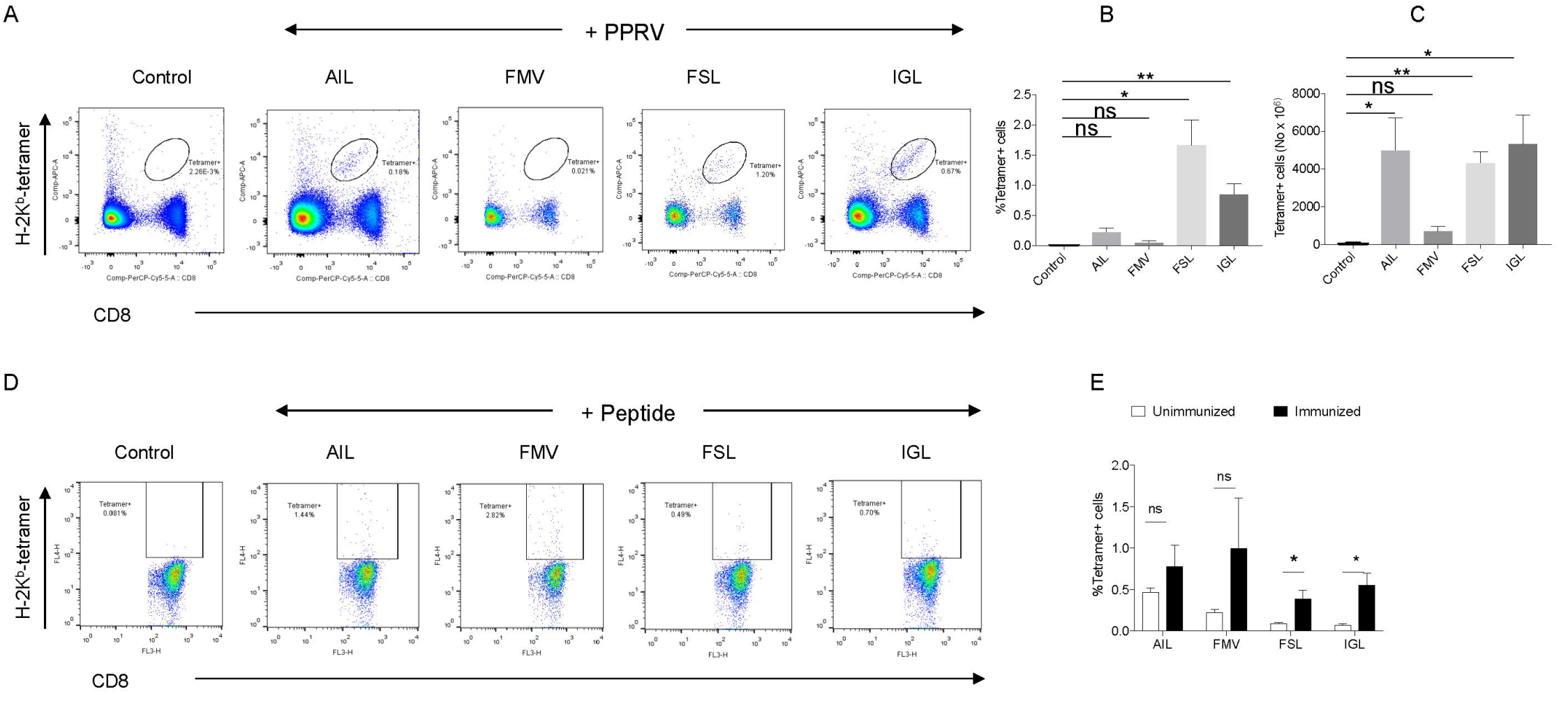
A
+ PPRV
Control
AIL
FMV
FSL
IGL
H-2Kb-tetramer
CD8
Tetramer+ 2.26E-3%
Tetramer+ 0.18%
Tetramer+ 0.021%
Tetramer+ 1.20%
Tetramer+ 0.67%
B
%Tetramer+ cells
ns
*
**
C
Tetramer+ cells (No x 10⁶)
D
+ Peptide
Tetramer+ 0.081%
Tetramer+ 1.44%
Tetramer+ 2.82%
Tetramer+ 0.49%
Tetramer+ 0.70%
E
Unimmunized
Immunized
%Tetramer+ cells